Available online at www.sciencedirect.com
SCIENCE DIRECT®
International Journal of Thermal Sciences 45 (2006) 217–236
International Journal of Thermal Sciences
www.elsevier.com/locate/ijts

Heat transfer and bubble formation in pool boiling: Effect of basic surface modifications for heat transfer enhancement

Stephan Kotthoff [a], Dieter Gorenflo [a,*], Elisabeth Danger [b], Andrea Luke [c]

[a] *Thermodynamik und Energietechnik, Universitaet Paderborn, D-33098 Paderborn, Germany*
[b] *Benteler Automobiltechnik GmbH, Paderborn, Germany*
[c] *Institut fuer Thermodynamik, Universitaet Hannover, Germany*

Received 1 June 2004; received in revised form 14 January 2005; accepted 14 January 2005

Available online 10 October 2005

Abstract

The present project within the joint research program on fundamentals of boiling heat transfer aims at better understanding of the basic processes which produce heat transfer enhancement in nucleate pool boiling. In the experiments, heater surfaces with two kinds of modifications for enhancement in the form of macro cavities with comparatively simple shapes are used in order to link experimental results of bubble formation and heat transfer to the geometric features of the cavities without additional assumptions, and particularly to resolve their overall effect on heat transfer into local convective or evaporative contributions without introducing severe simplifications.

The very accurate results on local heat transfer obtained so far around the circumference of the horizontal test tube with and without macro cavities for enhancement, and their combination with the local events connected to growing, departing and sliding bubbles are suitable to interpret the basic convective and evaporative processes which produce heat transfer enhancement in nucleate pool boiling.

Keywords: Heat transfer; Bubble formation; Pool boiling; Enhancement; Heater surface modification

1. Introduction

1.1. Related previous work of other researchers and of the authors

Within the joint research program on fundamentals of boiling heat transfer presented in this special issue, the project discussed here tries to contribute to better understanding of the basic processes which produce heat transfer enhancement in nucleate pool boiling. Since the first high-performance heater surface configurations were patented in the late 1960's, a great variety of evaporator tubes with enhanced surfaces have been developed, that can be divided in two main groups, one based on integral-fin tubes with modified fins to form reentrant grooves or tunnels ("structured surfaces"), see Fig. 1, and another based on plain tubes with sintered porous metallic matrix bonded to the tube surface ("porous surfaces"), see the example in Fig. 2.

A great number of experimental investigations of enhanced pool boiling heat transfer have been reported in the literature, see e.g. the reviews in [4–8]. Most of those measurements were performed, however, at saturation pressures p_s near atmospheric, and the correlations developed on the basis of the experimental results—also several containing a physical model of enhanced heat transfer fitted to the particular geometric configuration of the heating surface—mainly use the data gained at atmospheric pressure, but claim applicability in a broader sense, see, e.g. [9–20]; very detailed, but highly complex models have been developed recently by Chien and Webb [21] and Liter and Kaviany [22].

A good and comprehensive example of experimental results for pool boiling heat transfer at pressures near atmospheric from different structured or porous surfaces has been taken from Memory et al. [3] in Fig. 3. The data for refrigerant R114 ($CF_2Cl{\cdot}CF_2Cl$) exhibit the typical improvement of heat transfer from *structured* surfaces over plain tubes, with heat transfer coefficients α being higher by a factor of three to five at low heat fluxes q for modified integral-fin tubes (see the dashed lines

* Corresponding author. Fax: +49 5251 60 3522.
E-mail address: digo@thet.upb.de (D. Gorenflo).

1290-0729/$ – see front matter
doi:10.1016/j.ijthermalsci.2005.01.011

Nomenclature

d	bubble diameter	mm
D	tube diameter	mm
N	number of bubbles or active nucleation sites per analyzed area or time interval, 1/seq, 1/area	
N/A	density of active nucleation sites	cm^{-2}
p	pressure	bar
p^*	reduced pressure, $= p_s p_c^{-1}$	
P_a, R_a	arithmetic mean roughness height acc. to DIN EN ISO 4287 (P_q, P_p, $P_{p,m}$, P_t, P_z (μm) = other standardized roughness parameters)	μm
q	heat flux	$kW{\cdot}m^{-2}$
t	time	ms
T	temperature	°C
ΔT	superheat	K

Greek symbols

α	heat transfer coefficient	$kW{\cdot}m^{-2}{\cdot}K^{-1}$
Δ	difference	
φ	azimuthal angle	°

Characteristic parameters

Nu	Nusselt number
Gr	Grashof number
Pr	Prandtl number

Subscripts

A	at detachment
a, OD	outer diameter
B	bubble
c	in the critical state
cum	cumulated for an extended time interval, typically 500 ms
el	electrical
fpi	fins per inch
K	at the base of fins
lam	laminar
loc	local
m	mean
min	minimum
s	in the saturated state
sim	simultaneously ≡ within time interval of 1 ms between succeeding high speed video frames

for several types of GEWA-finned tubes). The improvement by the *porous* surface (High Flux tube) and the Thermoexcel-HE, Turbo-B tubes, (solid lines) is much better, but their α, q-behaviour is entirely different, thus ending up with basically the same heat transfer coefficients for all kinds of surfaces at high heat fluxes near 100 $kW{\cdot}m^{-2}$.

Investigations with Propane, Propylene and several refrigerants boiling on structured tubes in a wide pressure range (up to 50% of the pertaining critical pressures p_c) reveal significant deviations from the rather uniform increase of α with q for the structured tubes at atmospheric pressure in Fig. 3. In the case of GEWA-TX tubes, in particular,

(a) α-values are much higher than expected and almost do not increase with q at high reduced pressures p_s/p_c and small heat fluxes, and
(b) at low pressures p_s/p_c and high heat fluxes, α becomes independent of pressure and heat flux,

see the data in Fig. 4 (from [1]) at $p^* = p_s/p_c = 0.147$ (a) and p^* from 0.055 to 0.147 (b). Both effects could be explained using photos of bubble formation: In the first case, stable vapour–liquid interfaces bridge the narrow gaps of 0.23 mm (see Fig. 1) between the tops of neighbouring fins at the top of the (horizontal) tube and trap vapour in the tunnels between the fins, and in the second case, heat transfer is dominated by the restricted release of the great amount of vapour produced in the tunnels at high heat flux, similar to single-phase forced convective heat transfer which is independent of heat flux and pressure, while at the highest pressure in Fig. 4, nucleation exists all over the tube surface and α increases with q and p^*, also at the highest heat flux investigated (for more details, see [6,23]).

Both peculiarities also occurred with Propylene and refrigerant R134a ($CF_3{\cdot}CH_2F$) boiling on the TX-tube, while the first effect (a) was not found with another refrigerant (R152a, $CHF_2{\cdot}CH_3$) within the same ranges of q and p^* [1,24–26]. The latter also holds for all fluids investigated with the GEWA-YX tube, and the second effect (b) was less pronounced with these tubes, obviously because of the somewhat wider gaps between the fins (0.34 mm) and their different shape (see Fig. 1).

Fig. 5 demonstrates that pressure dependencies of the heat transfer coefficient α_{OD} for various types of structured surfaces may differ significantly from each other, also within the range of intermediate heat fluxes ($q_{OD} = 20$ $kW{\cdot}m^{-2}$), and that enhancement vanishes at high reduced pressures p^*. Fig. 5 from [27] has been supplemented by data from Fig. 6 for a porous surface showing that its superiority to the structured surfaces disappears at high reduced pressures in a similar way as with increasing heat flux at constant pressure for the other porous surface in Fig. 3.

Measurements with Propane boiling on a CuNi-tube (8 mm OD) with aprox. 300 μm thick, plasma sintered Ni-based porous layer are presented in Fig. 6 as example of heat transfer from porous surfaces over an extended range of reduced pressures (and heat fluxes) [28]. The porous layer was manufactured at DLR-Institute of Thermodynamics, University of Stuttgart, and the tube was assembled in Paderborn and tested in the apparatus and in between the experiments of this paper.

The data show a systematic increase of heat transfer coefficient α with heat flux q and reduced pressure p^* which

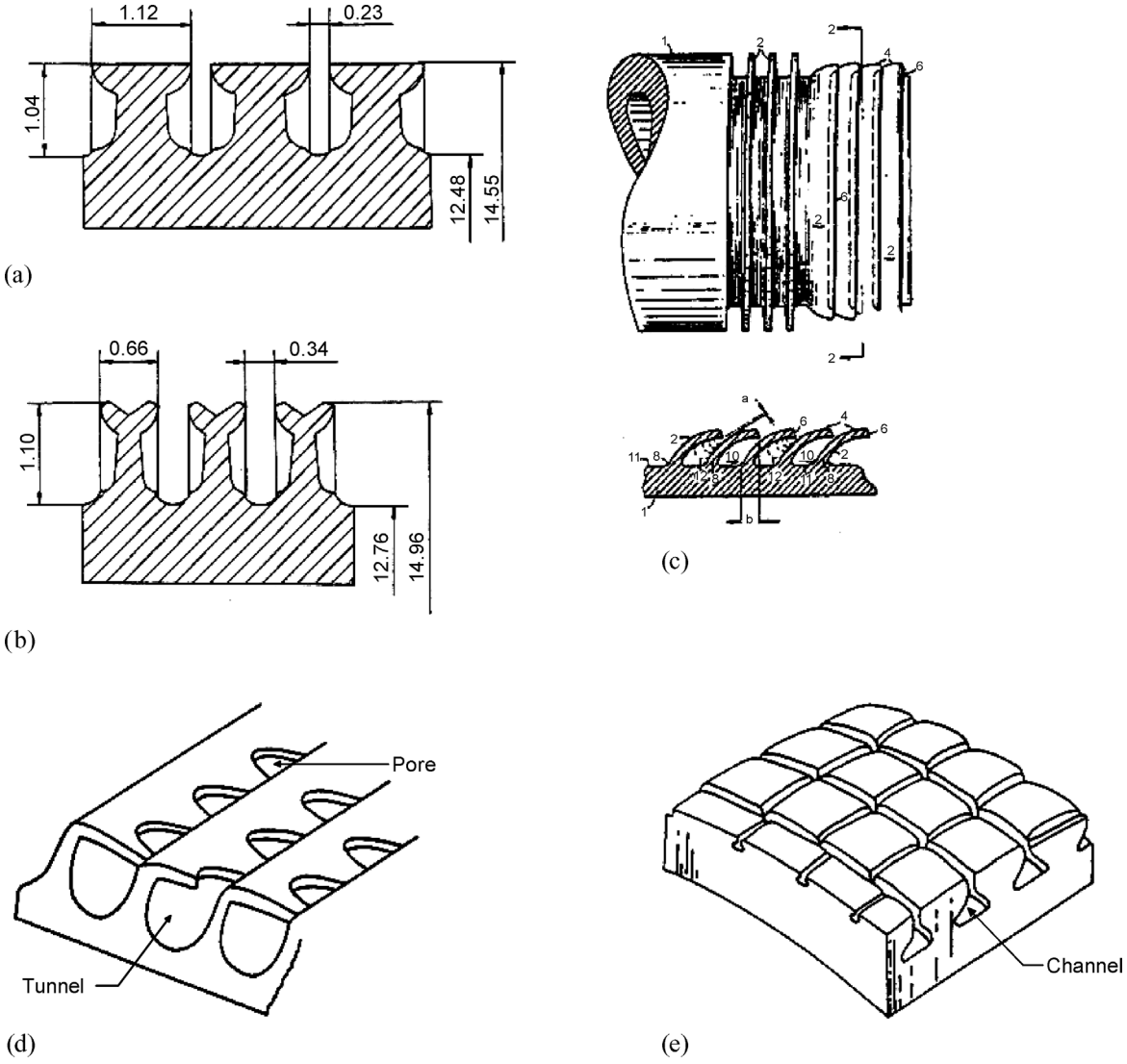

Fig. 1. Examples of structured tubes: (a) Finned tube with flattened tips: GEWA-TX (from [1]); (b) Finned tube with notched tips: GEWA-YX (from [1]); (c) Finned tube with bent tips (from [2]); (d) THERMOEXCEL-HE tube (from [2]); (e) TURBO-B tube (from [5]).

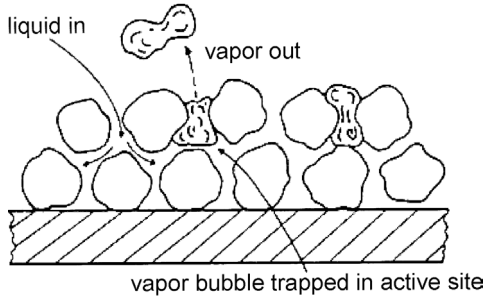

Fig. 2. Example of tubes with sintered porous (metallic) surface (schematic; from [2]).

ends at an upper boundary with α-values being independent of p^* and slightly decreasing with increasing heat flux. The same decrease has been found in [22] for n-Pentane boiling at atmospheric pressure ($p^* = 0.03$) on a uniform porous layer coating, only shifted to q-values approx. 5 times higher (α decreasing from approx. 40 to 23 $\mathrm{kW \cdot m^{-2} \cdot K^{-1}}$ for q increasing from 142 to 460 $\mathrm{kW \cdot m^{-2}}$).

As in the case of effect (b) discussed for the GTX-tube in Fig. 4, heat transfer at the boundary obviously is limited by the maximum amount of vapour that can be released from the pores of the surface layer and by the reflux of liquid that is sucked in. The onset of this process progresses to lower heat fluxes when the thermodynamic critical state is approached, because the density difference between liquid and vapour, and the surface tension—which are the driving forces, become continuously smaller. Although this boundary does not correspond to the burnout condition, an analogy can be seen to the vanishing burnout heat flux at high and approximately constant α-values on plain tubes near the critical state [29].

From the comparison with new measurements of pool boiling heat transfer on a plain copper tube with 8 mm OD (dashed straight lines in Fig. 6 [30]), similar decrease of enhancement factors with rising heat flux q and reduced pressure p^* follows as for structured surfaces, starting, however, at higher factors of approx. 10. At 50% of p_c and the highest heat flux investigated, enhancement is vice versa already, and the *plain tube* is

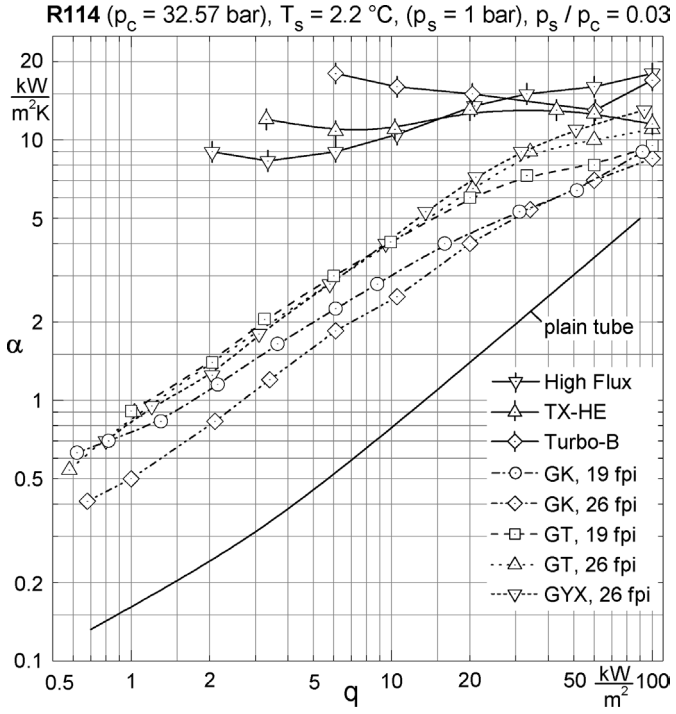

Fig. 3. Example of experimental results for pressures near atmospheric: Double logarithmic plot of heat transfer coefficient α as function of heat flux q for refrigerant R114 boiling on different structured and porous surfaces (from [3]).

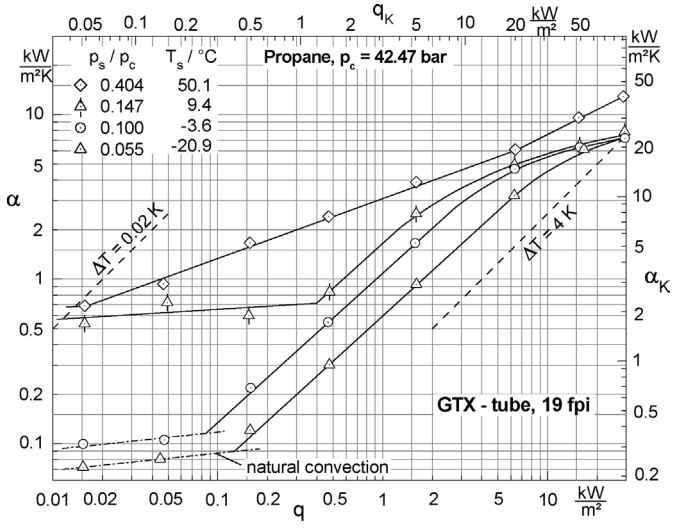

Fig. 4. Heat transfer from a structured tube (GTX, Fig. 1) to Propane at different pressures. α, q-related to total wetted surface of the tube; α_K, q_K-related to surface of the (plain) tube at base of fins (from [1]).

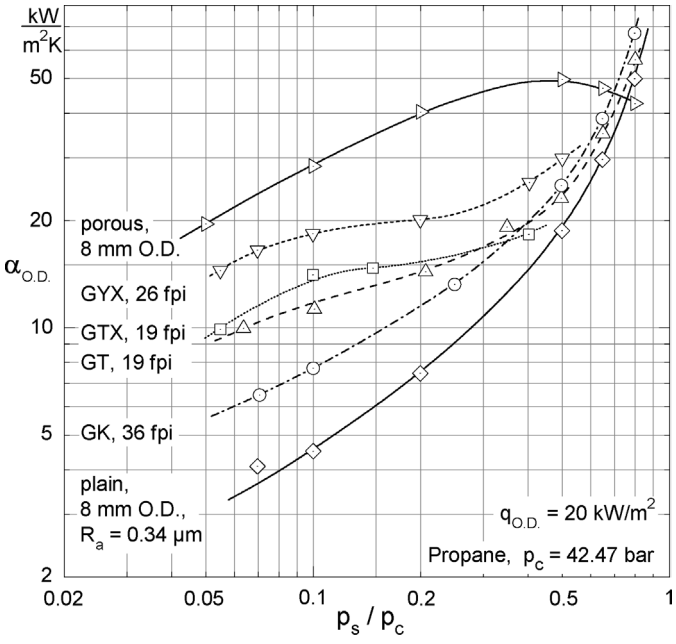

Fig. 5. Pressure dependence of heat transfer coefficient at constant intermediate heat flux for different structured tubes and comparison with a plain tube (from [27]) and with the porous tube of Fig. 6. $\alpha_{O.D.}, q_{O.D.}$-related to surface of plain tube with D corresponding to fin tips.

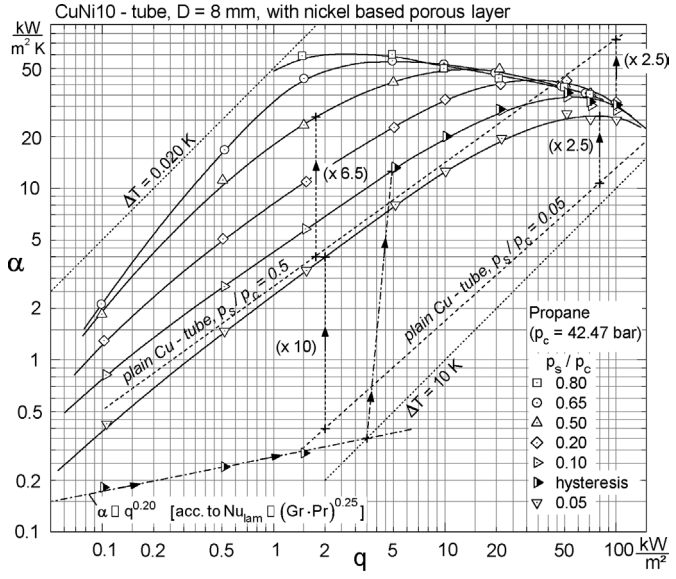

Fig. 6. Heat transfer from a copper-nickel tube with porous surface to Propane boiling in a wide range of (reduced) saturation pressures (from [28]) and comparison with a plain Cu-tube (8 mm OD; from [30]).

better by the same factor (2.5) as the porous at 5% of p_c and approximately the same heat flux. (Comparison with a plain tube made from *copper* does not reduce accuracy, because pool boiling heat transfer is almost identical for Cu or CuNi10 at the same reduced pressures p^* and for the same surface roughness in both cases, as has been shown in [31] for tubes with approx. 25 mm OD in the same pressure range.)

For $p^* = 0.10$, delayed onset of nucleation is demonstrated at a test run with *increasing* heat flux (symbols: partly solid triangles), and the threshold of wall superheat $\Delta T = 10$ K is within the range found for smooth tubes at similar reduced pressures (see, e.g. [32–34]; in the present case, bubble formation started during the comparatively fast increase of q from 1.5 kW·m^{-2}, shortly before the next value of 5 kW·m^{-2} to be stabilized was reached, therefore the dot-dashed line has been drawn somewhat inclined). For recent discussion of hysteresis effects on porous surfaces see also [35].

The measurements at the highest reduced pressures—always taken with *decreasing* heat flux—indicate that the superheat of the wall *increases* again at small heat fluxes, although the

electrically supplied heat input *is diminished* to the smallest values investigated, cf. the circle and triangle on their bases at $q = 0.1$ kW·m^{-2} in Fig. 6, or better to be recognized in the (explicit) $q, \Delta T$-representation of Fig. 7. This may be due to the fact that favourable micro paths for vapour release from the porous matrix to the surface will die down because the vapour content trapped within the matrix (similar to effect (a) in Fig. 4) is decreasing (ΔT being defined as superheat of the wall at the *inner* boundary of the porous layer).

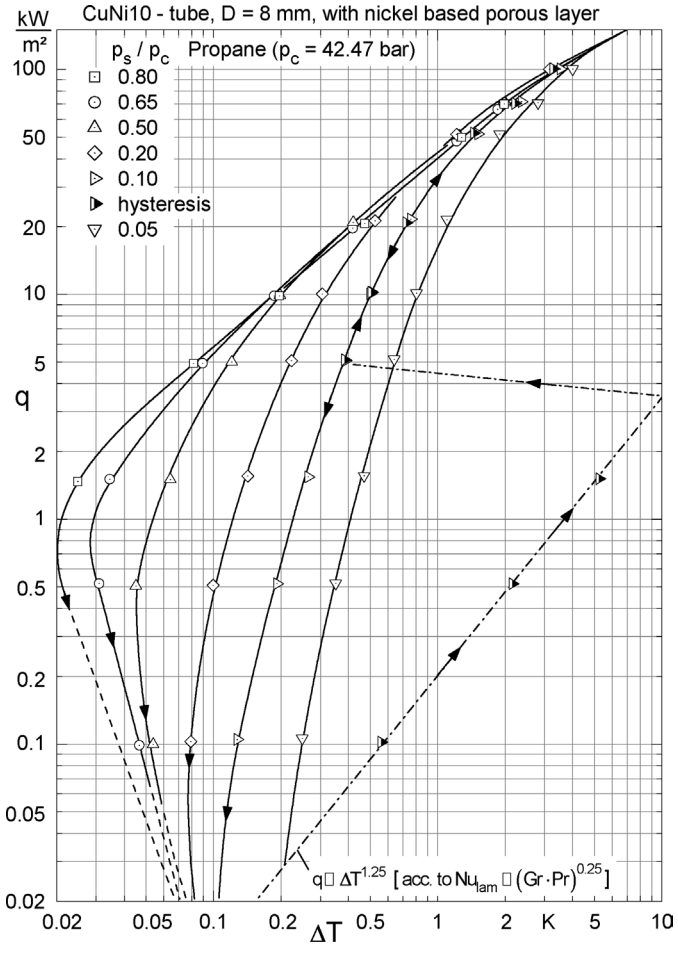

Fig. 7. Representation of heat flux q over wall superheat ΔT for the data of Fig. 6.

1.2. Brief introduction of the present research

The representative examples of pool boiling heat transfer from enhanced surfaces selected above demonstrate how difficult it would be to develop calculation methods for the prediction of enhanced boiling heat transfer from any of the complex commercially used surface configurations, particularly if wide ranges of heat flux and (reduced) pressure are to be included and if extrapolation to configurations other than the one experimentally investigated is required.

Therefore, the scope of the subproject presented in the following is restricted to the investigation of a heater surface with two kinds of modifications for enhancement in the form of macro cavities with comparatively *simple shapes* in order to link experimental results of bubble formation and heat transfer to the geometric features of the cavities without additional assumptions, and particularly to resolve their overall effect on heat transfer into local convective or evaporative contributions without introducing severe simplifications.

The cavities were rolled on the tubes by Fa. Wieland, Ulm, Germany, in rows at distances of approx. 200 μm and with the largest dimension of the cavities oriented parallel to the tube axis. In Fig. 8 (from [36]), topographies of the surface structures (on the copper tube) are shown in a photo realistic representation (bottom) and with the depths of the cavities indicated by colours (top). The topographies were taken by a stylus instrument within another subproject of the research group which is dedicated to the analysis of size and position of the *micro* cavities within the roughness structure of the various heating elements used within the joint program (for more details see the paper by Luke on surface measurement in this issue).

Two kinds of cavities were applied to be tested simultaneously, the cavities of the simpler “secondary structure” being

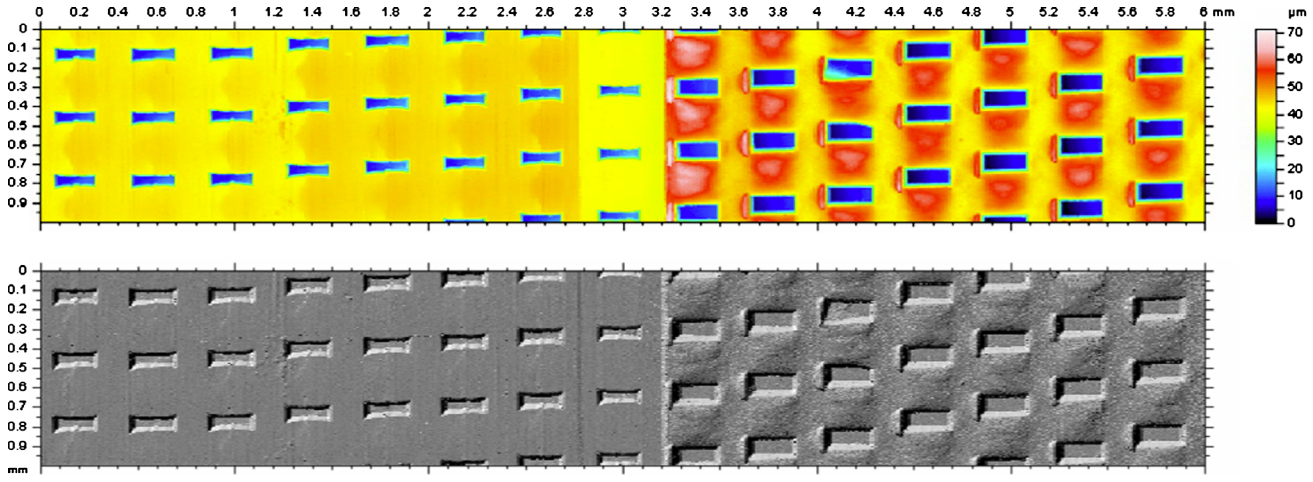

Fig. 8. Topography of the copper tube (near borderline of the two surface structures) in a quasi-photo realistic representation (bottom) or with the depths of the cavities indicated by colours (top; from [36]).

purely radially oriented in depth (size: approx. 200 × 100 × 50 μm, see Fig. 8, on the right). The cavities of the "main structure" with reduced mouth width (Fig. 8, on the left) were modified in a second rolling step in order to produce reentrant effects, the microstructure of the surface roughness on the areas between the macro cavities, however, having been flattened significantly during the second step (see Section 3).

Refrigerant R134a and 2-Propanol (and also Propane in some cases) were selected as test fluids because their vapour pressure varies over a wide range of reduced pressure p^* within the temperature range covered by the experimental apparatus. Heating elements are single, horizontal copper or copper-nickel tubes (CuNi10; exact type: CuNi10Fe1.6Mn) powered by dc-resistance heaters and with diameters at the upper limit of common technical evaporator tubes (Cu: 25.4 mm; CuNi: 24.0 mm) to increase convection by the swarm of rising bubbles. Thus, local convective and evaporative effects of the bubbles sliding upwards along the wall are detected more clearly than with tubes of small diameters (cf. e.g. [37–40]).

36 miniaturized thermocouples (0.25 mm OD) were equally distributed over two cross-sections of the copper tube, axially shifted against each other by 30 mm (see Fig. 9, to scale) to monitor circumferential temperature variations within the two domains with different surface modifications (axial positions of the thermocouples differing somewhat due to length uncertainties during the soldering process, see [31]).

In the experiments, a new, slightly modified version of the so-called standard apparatus for pool boiling heat transfer measurements is used which is described in detail in [31,41], together with the outlines of the experimental procedure. Combined with the heat transfer measurements, bubble formation is recorded by photographs and by a high speed digital video system (Fa. Weinberger, Karlsruhe, Germany) for up to 1000 images per second with a resolution of 512 × 512 pixels. The densities (numbers and exact local positions) of nucleation sites (N_{sim}) active simultaneously (i.e. within the time interval of 1 ms) or alternately (N_{cum}), the rate of bubble release from each site (N_B), the (equivalent) diameters d_A of the bubbles at detachment from the sites, and the increase of the diameters d_{B} for the bubbles sliding upwards along the tube wall are evaluated by semi-automatic methods. For detailed descriptions of these methods, see [31,42–44].

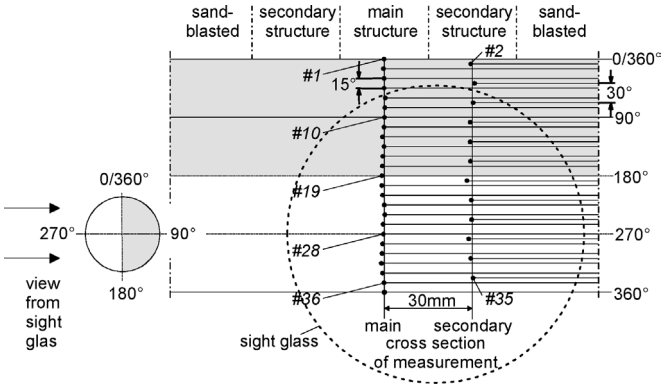

Fig. 9. Positions of the thermocouples within the two cross sections of measurement (to scale).

2. Summary of results without modifications and for first modified surfaces

2.1. Local heat transfer

Variation of local wall superheats ΔT with azimuthal angle φ, heat flux q (at $p^* = \mathrm{const}$; on the left) and reduced pressure p^* (at $q = \mathrm{const}$; on the right) is demonstrated in Fig. 10 for Propane, 2-Propanol and R134a boiling on the fine sandblasted Cu-tube *without surface modifications* [31]. As can be seen, a minimum in ΔT is developed for intermediate heat fluxes or intermediate (and up to comparatively high) reduced pressures, caused by evaporative and convective effects of the bubbles growing at active nucleation sites on the lower parts of

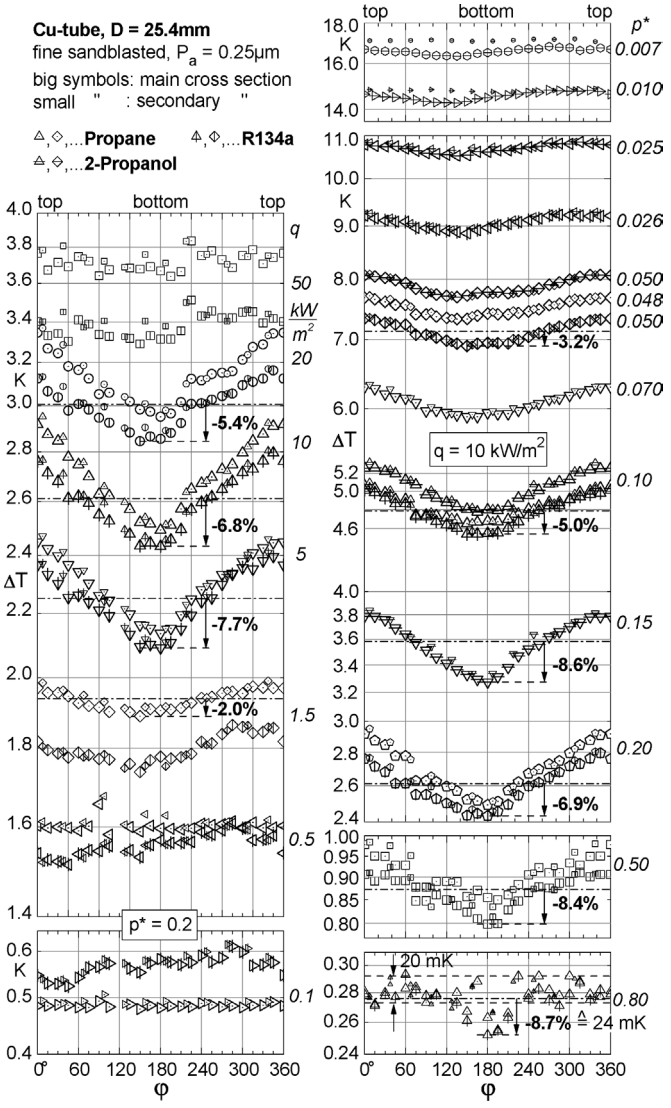

Fig. 10. Variation of local wall superheats ΔT with azimuthal angle φ, heat flux q (at $p^* = \mathrm{const}$; on the left) and reduced pressure p^* (at $q = \mathrm{const}$; on the right) for Propane, 2-Propanol and R134a boiling on the fine sandblasted Cu-tube ($P_a = 0.25$ μm) without surface modifications (from [31]).

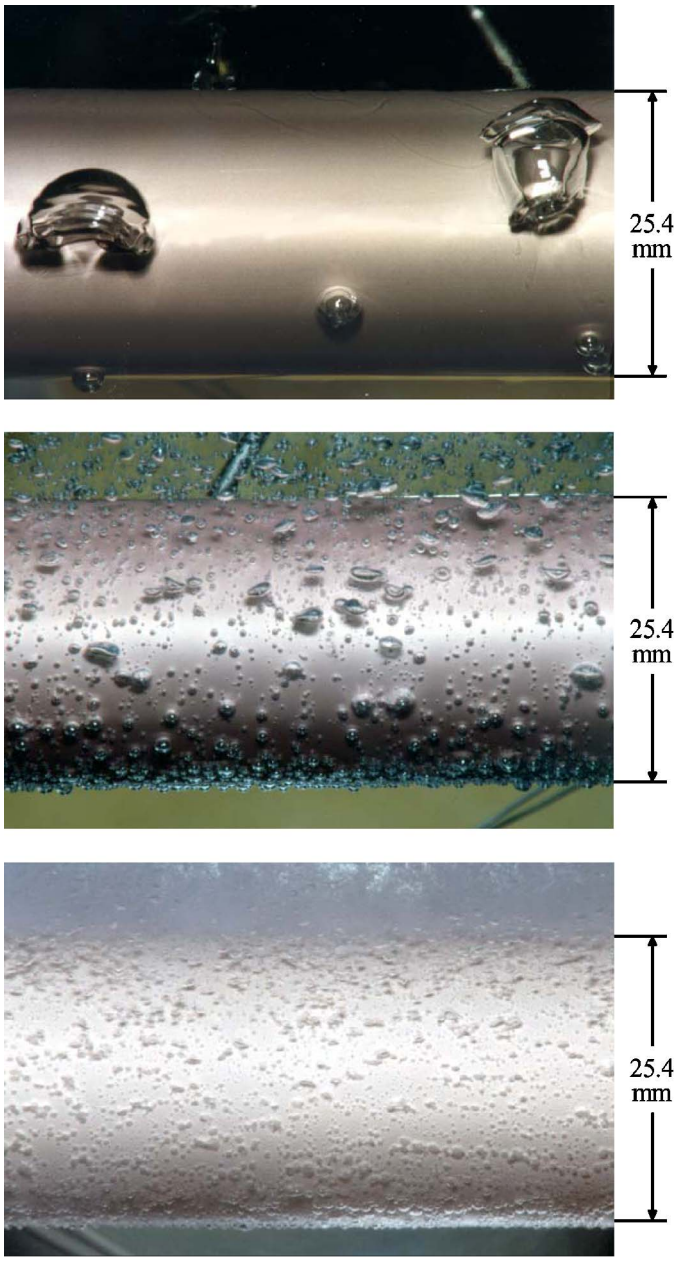

Fig. 11. Bubble formation on the fine sandblasted Cu-tube without macro cavities at constant, intermediate heat flux $q = 10$ kW·m^{-2} and different reduced pressures. Top: $p^* = 0.010$; middle: $p^* = 0.15$; bottom: $p^* = 0.80$.

the tube wall and sliding upwards along the superheated liquid layer near the wall. These effects are gradually loosing importance,

- if the density of active sites becomes high (high q-values) or number of bubbles becomes small (small q-values), see Fig. 10 on the left, and
- if reduced pressure p^* is very low, with big bubbles and small number of active sites, even at intermediate q-values, or if p^* is very high, with tiny bubbles, high site density (even at small q-values) and vanishing buoyancy, see Fig. 10 on the right, in combination with the photos of bubble formation in Fig. 11.

The systematic $\Delta T, \varphi$-behaviour *within* each of the two cross sections of measurement and the small (or non-existent) deviations *between* the two cross sections (big or small symbols in Fig. 10) indicate that heat transfer conditions within the inner structure of the test tube are homogeneous—an important prerequisite for correct interpretation of circumferential variations of the wall superheat ΔT. The systematic differences developing between the two cross sections of measurement at the three lowest reduced pressures (cf. small and big symbols in Fig. 10, on the right at $\Delta T = 11$ K and more) will certainly be caused by differences in local positions of the very few, simultaneously active sites existing under these conditions (see Fig. 11, top) and by differences in their specific activation behaviour. In the same way, most of the ΔT-scatter for the highest heat flux (50 kW·m^{-2}) or at the lowest superheat (0.28 K) will be initiated by local irregularities of bubble formation distributed at random, as can be concluded from a comparison with the corresponding data in Figs. 22 and 24 ($p^* = 0.2$, 50 or 70 kW·m^{-2}) or in Fig. 26 ($p^* = 0.8$, 10 kW·m^{-2}, 0.28 K), where the more regular bubble formation at the equally distributed macro cavities 'smoothes' the $\Delta T, \varphi$-curves quite significantly.

In Fig. 13, characteristic examples of the reduction of wall superheat are shown which has been achieved by the *macro cavities for heat transfer enhancement*. An impression of the regular form of the cavities within the first main macro structure on the Cu-tube is given in Fig. 12 by four selected topographies. Comparing the (almost) entirely identical shapes of the cavities at different positions around the tube surface reveals that the structure had been applied without any circumferential irregularities (in fact, the structure produced in a first attempt had not been satisfactory and had been removed again).

Reduction of superheat ΔT by the macro cavities is significant, as can be seen in Fig. 13, particularly at intermediate reduced pressures or intermediate and down to low heat fluxes, respectively, that means under conditions where heat transfer is influenced most by local bubble formation—also *without* macro cavities.[1] The differences between the results for the two kinds of macro cavities, however, are not very pronounced (small and big symbols with cross) indicating that perhaps mouth width of the main cavities should have been reduced to a higher extent. (The different surface roughness within the main or secondary macro structure *between* the cavities may also be of influence, see discussion of Fig. 18, and Section 3). The overall improvement of the average heat transfer coefficient achieved by the macro cavities is up to approx. 35% for the secondary and up to approx. 45% for the main structure. For more results about average and local heat transfer from the first modified surfaces

[1] In comparison with Fig. 11, it can be observed that the defective thermocouple at $\varphi = 120°$ had been 'bridged' by the arithmetic mean of the two neighbouring thermocouples in the diagram from [36] (see big open symbols). During the handling process prior to the heat transfer measurements with the first macro structure—applying and removing the preliminary macro structure, then applying the first, and in between: sandblasting 3×, roughness measurements 3×, cleaning, transport etc.—5 more thermocouples of the main structure and 5 of the secondary became defective, cf. the remaining 18 big or 7 small symbols with cross in Fig. 13.

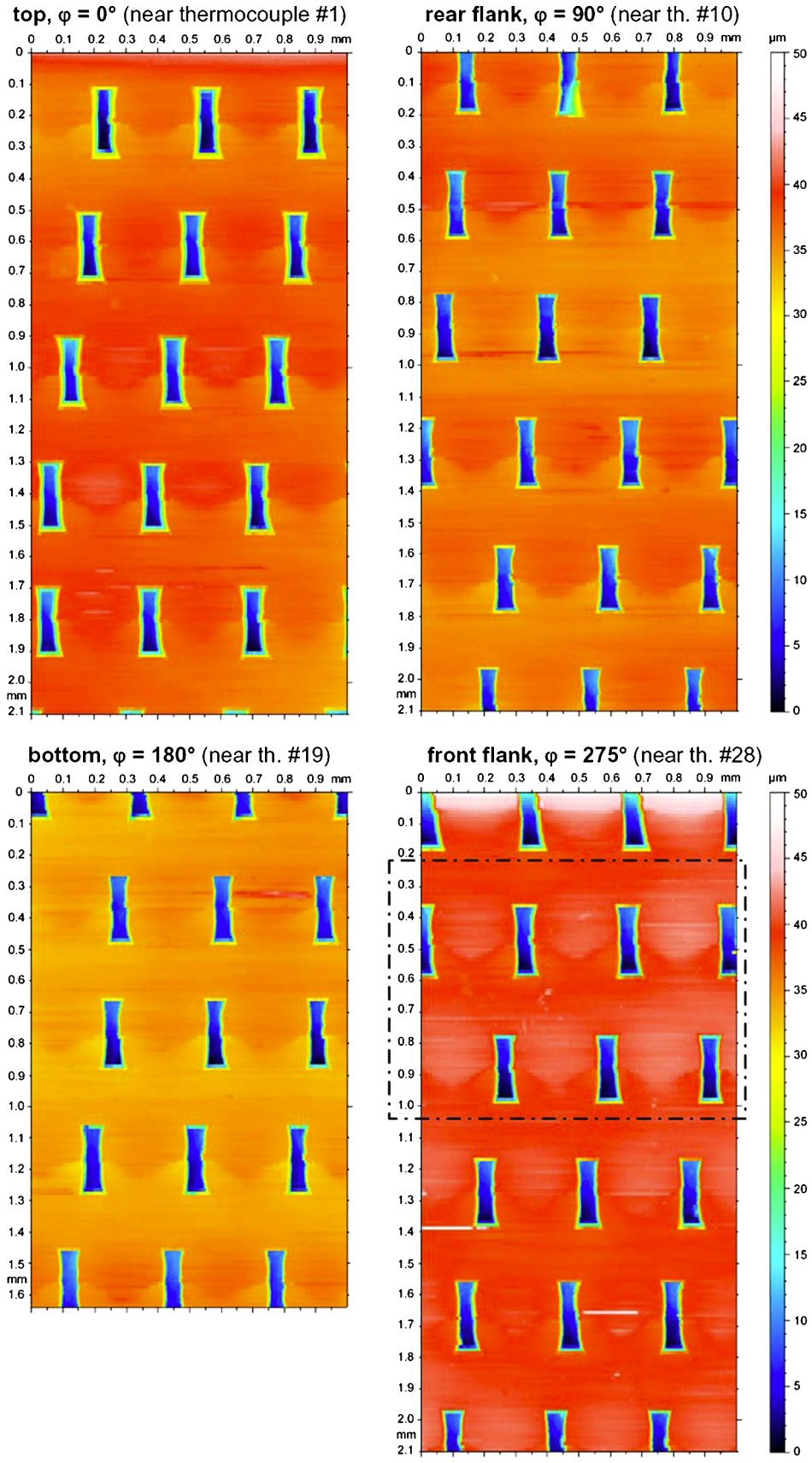

Fig. 12. Surface topographies of the first macro structure on the Cu-tube at selected azimuthal positions (0°, 90°, 180°, 275°, near thermocouples # 1, 10, 19, 28, see Fig. 9).

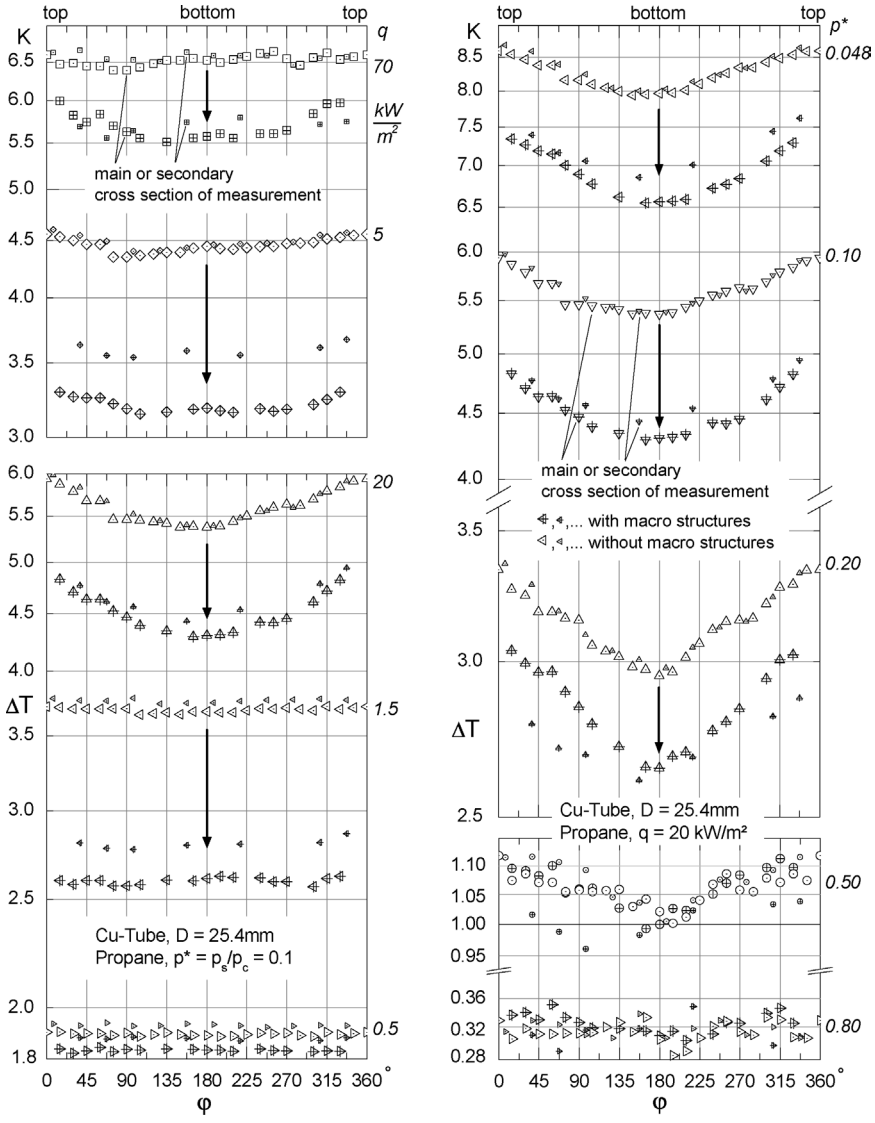

Fig. 13. Comparison of local wall superheats ΔT for Propane boiling on the fine sandblasted Cu-tube without and with macro cavities for heat transfer enhancement (from [36]). Parameter: Left: Heat flux q at constant (intermediate) reduced pressure $p^* = 0.10$ Right: Reduced pressure p^* at constant (intermediate) heat flux $q = 20\ \mathrm{kW{\cdot}m^{-2}}$.

see the comparison with the new modifications in Section 3 (and [36,45]).

2.2. Bubble formation

Much less systematic investigations exist on bubble formation than on heat transfer for evaporator surfaces with dimensions and roughness structures relevant in practice, as a review of the literature on interactions between heat transfer and bubble formation in nucleate boiling given in 1998 [23] revealed. Therefore, much more *basic investigations* on bubble formation than on heat transfer had to be carried out for the test tube *without modifications for enhancement* in the first stages of our research project, and new or existing methods for the analysis of bubble formation had to be developed or improved, respectively. The most important results which have been obtained so far on the densities N/A of active nucleation sites, the rate N_B/t of bubble release from each site and the diameter d_A of the bubbles at detachment, will be summarized in the following; a more detailed description is given in two recent publications [31,44].

In the first place, it has to be pointed out that the activation behaviour of *micro* cavities within the roughness structure of evaporator surfaces, to become active nucleation sites for the production of vapour bubbles, may vary tremendously, even under boiling conditions with very thoroughly stabilized values of electrical energy input to the heating element and of saturation temperature and pressure of the pool of liquid (as is the case for the experimental apparatus and procedure used in this project). This holds for all the characteristic parameters of bubble formation, like

- density of active nucleation sites on the heater surface,
- temporal activation behaviour of each site, and
- size of the bubbles at detachment from the sites.

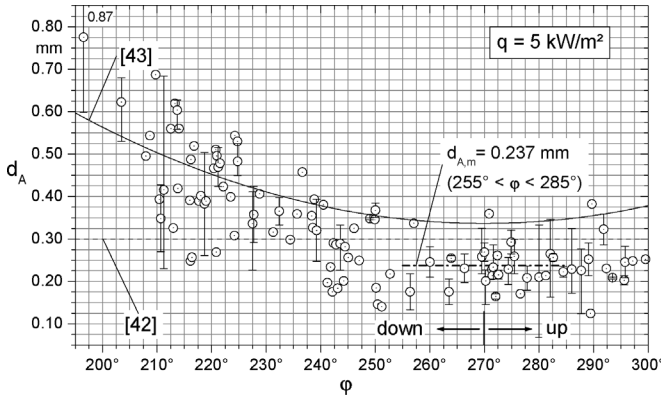

Fig. 14. Variation of bubble departure diameter d_A with azimuthal angle φ near the front flank of the fine sandblasted Cu-tube without macro cavities for Propane at $p^* = 0.1$, $q = 5$ kW·m^{-2}. Bars: Maximum variation of data at constant boiling conditions (from [31]).

The main reason for this scatter are short-time reductions of the superheat at a cavity ready to be activated, by (one or more) cavities *active* already in its *immediate* neighbourhood or by a bubble sliding over the cavity, see e.g. the detailed history of 11 active sites recorded in [31,44] and the papers by Kenning on liquid crystal thermography [46–48]. The first effect is particularly pronounced for surfaces sandblasted by grain with comparatively uniform particle sizes which produces many similar cavities in a very homogeneous surface structure as has been the case for the 25.4 mm Cu-tube with fine sandblasted surface (mean roughness: $P_a = 0.25$ μm) before applying the macro structures for enhancement.

The scatter is shown in Figs. 14–16 by typical examples for N/A, N_B, d_A. As can be seen, the values of the three parameters vary for the pertaining, *constant boiling conditions* between

- 0.07 and 0.87 mm for d_A (Fig. 14)
- 1 and 11 or 1 and 38 per 500 ms for N_B (Fig. 15) and
- 1 and 11 on 51.42 mm^2 for $N_{\mathrm{sim,1\ ms}}$ (Fig. 16).

This demonstrates that great care has to be taken when average values of these parameters are used in models to calculate the heat transfer performance of an evaporator surface from bubble formation, as e.g. in the well-known combination of ideas from Mikic and Rohsenow [49], and Han and Griffith [50].

Variation of bubble departure diameter d_A with azimuthal angle φ for the new results is somewhat more pronounced than according to a correlation developed earlier ([51], solid curve in Fig. 14), and the d_A-values predicted by this correlation and a correlation of Weckesser [52] based on measurements of bubble formation on a horizontal plate (dashed) lie within the experimental scatter of the new data near the flank of the tube. As can easily be understood, the mean d_A-values near the flank of a horizontal tube become smaller with increasing heat flux, and the d_{A}, φ-dependence becomes weaker (and has already vanished at $q = 20$ kW·m^{-2}, see the more detailed discussion in [31]). For this and also for the other two parameters, it has to be taken into account, however, that difficulties of data processing for bubble formation increase with increasing heat flux and distance from the (front) flank of the test tube.

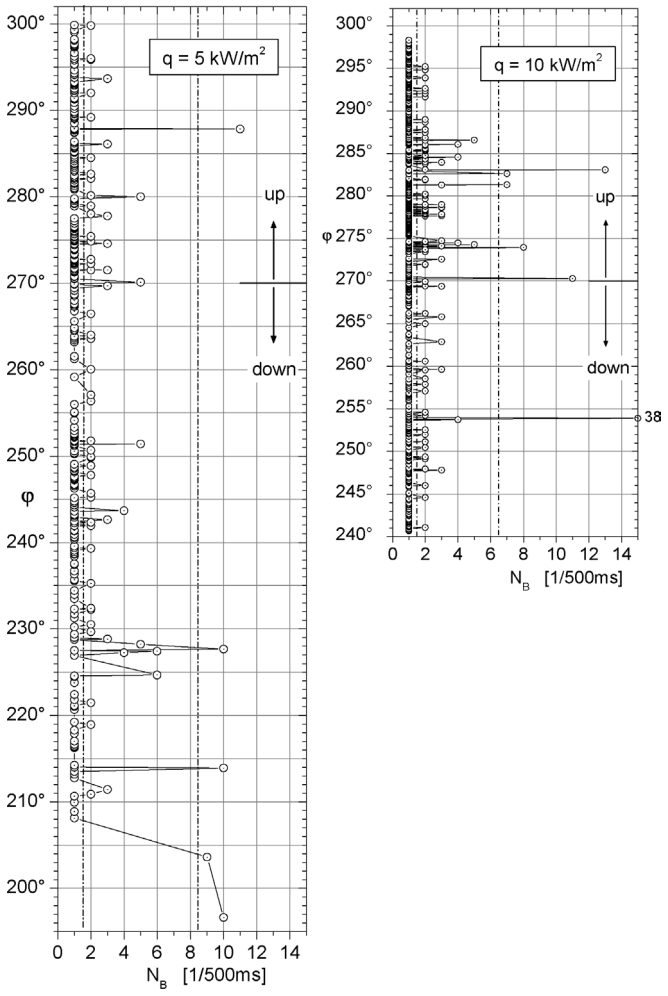

Fig. 15. Azimuthal distribution of active sites and number N_B of bubbles originating from each site during an entire video sequence of 500 ms (from [31]). Fine sandblasted Cu-tube without macro cavities, Propane at constant $p^* = 0.1$ and two heat fluxes.

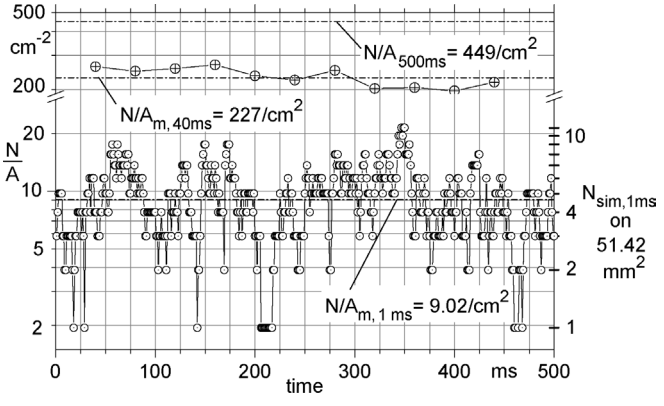

Fig. 16. Density $(N/A)_{\mathrm{sim,1\ ms}}$ of simultaneously active sites (time period: 1 ms; bottom) for an entire video sequence of 500 ms, and pertaining cumulative values for 40 or 500 ms (above). Fine sandblasted Cu-tube ($P_a = 0.25$ μm) without macro cavities; R134a, $p^* = 0.1$, $q = 10$ kW·m^{-2} (acc. to [44]).

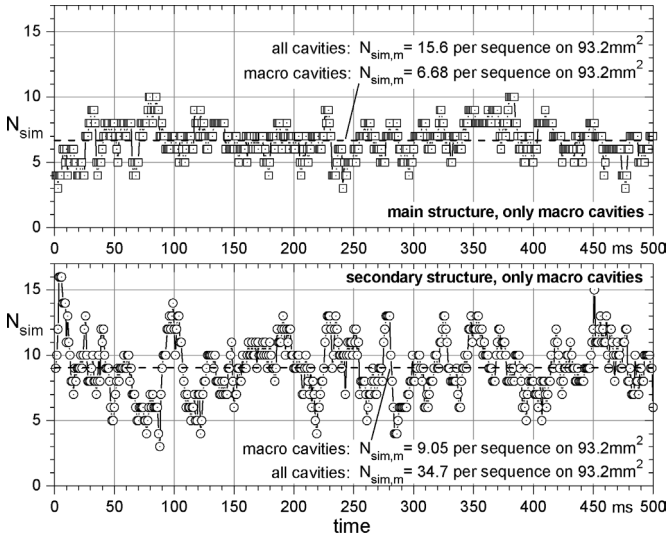

Fig. 17. Number N_{sim} of simultaneously (1 ms) active macro cavities at $q = 10\ \mathrm{kW{\cdot}m^{-2}}$ (symbols in shaded circles in Fig. 19) on the main or secondary structure, resp., during 500 ms (from [44]).

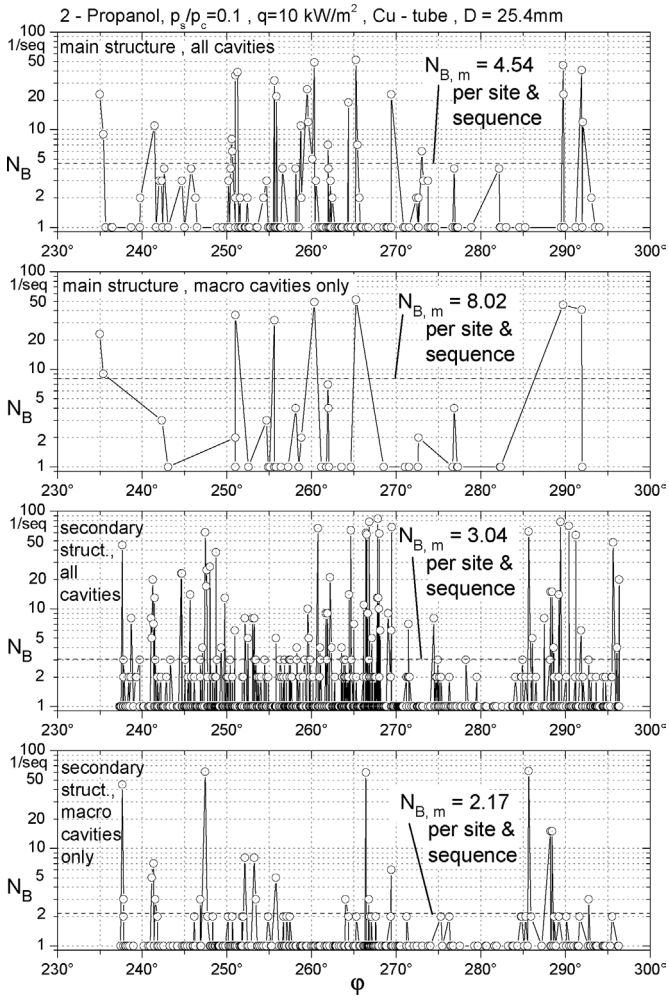

Fig. 18. Azimuthal distribution of active sites and number N_B of bubbles originating from each site on the main (diagrams at the top) or secondary (bottom) structure for the same conditions as in Fig. 17 (from [44]).

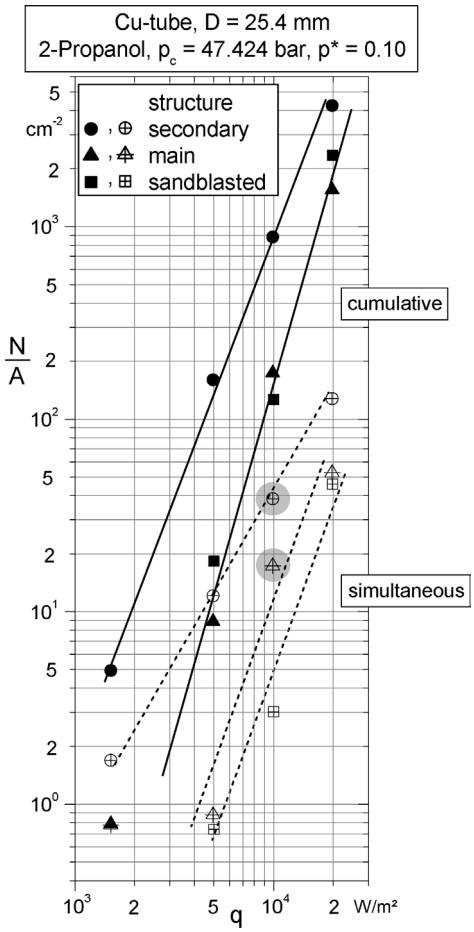

Fig. 19. Cumulative and simultaneous site densities N/A on the main or secondary structure, resp. as functions of heat flux q (from [44]), and comparison with the fine sandblasted Cu-tube without macro cavities (from [31]) for 2-Propanol at $p^* = 0.1$.

Examples of the different activation behaviour of individual sites near the flank of the tube are given in Fig. 15 for two heat fluxes at constant pressure. The data show that almost all the sites are active only once or twice within 500 ms and that bubble production rate is high for only a few of them. This means that activation is influenced for *most* of the sites—even at these comparatively low heat fluxes—either by neighbouring sites or by sliding bubbles via "site seeding", "premature detachment" or purely thermal interaction. As positions of sites at the same azimuthal angle φ may differ in axial direction, the diagram does not allow to conclude which of the mechanisms is responsible in each individual case; to do so, activation maps are necessary containing the exact local positions of neighbouring sites and their temporal activation behaviour during entire video sequences (see, e.g. the exemplary analysis for 11 sites in [31,44]).

An additional phenomenon which contributes to the great scatter of bubble formation data, is generated by the ensemble of bubble formation processes occurring on the tube surface simultaneously, see Fig. 16, at the bottom. The scatter for N_{sim} reveals an oscillating behaviour containing short-time fluctuations with time intervals of a few milliseconds between maximum and minimum value—corresponding to the mean growing

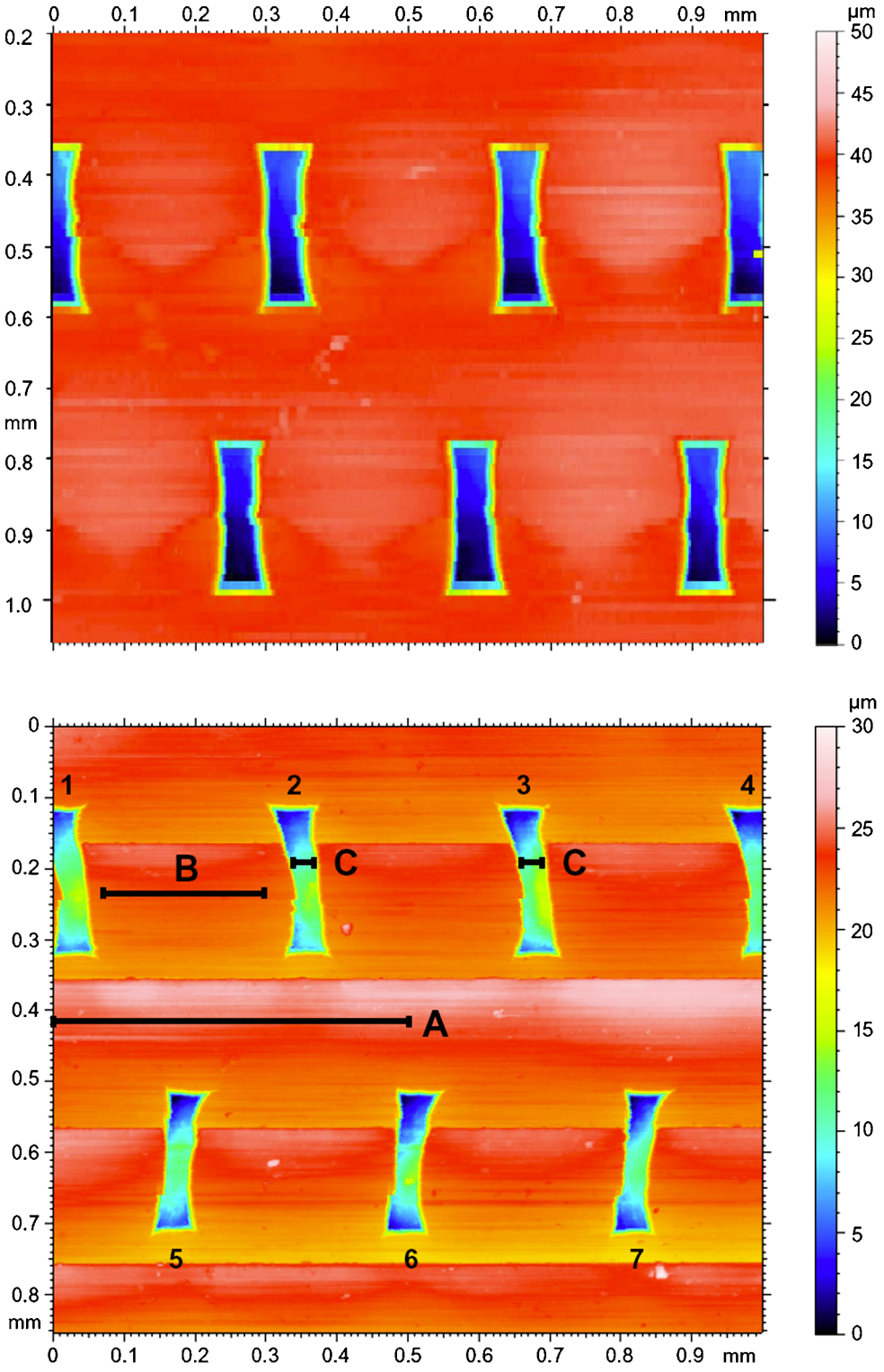

Fig. 20. Comparison of second main macro structure (bottom) with first (top = enlarged part of front flank, see $\varphi = 275°$ in Fig. 12); # 1–7 = number of macro cavity; A–C = location of roughness profiles given in Fig. 27.

periods of bubbles found under similar conditions [31,44]—, and superposed long-time fluctuations with roughly tenfold characteristic time intervals. Residual fluctuations of the thoroughly stabilized input of electrical energy to the test tube could definitely be excluded as a possible reason by oscilloscope analysis [53].

A plausible explanation has been offered in [44]: At those moments when only a few bubbles are produced, the heat removed may be lower than the *constant* electrical heat input, resulting in a rise of superheat. This in turn will activate so many sites that more heat is removed than added, and the superheat decreases again, but down to significantly *below* the

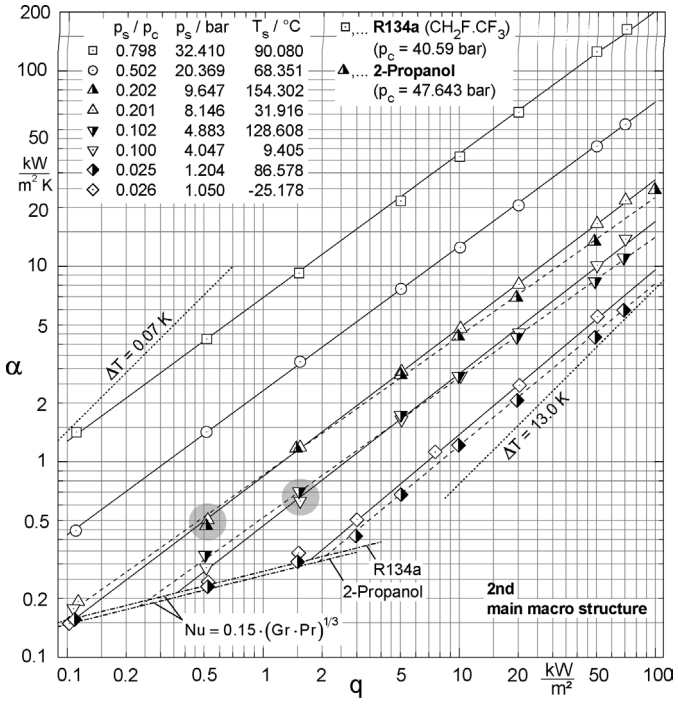

Fig. 21. Heat transfer coefficients α for R134a and 2-Propanol boiling on the Cu-tube with modified main macro structure at different heat fluxes q and reduced pressures p^*.

equilibrium value because the bubbles growing already, need less superheat than the average and will continue to grow for a few more milliseconds. It seems that the very same behaviour also occurs *with macro cavities* (see Fig. 17).

Consistent with the result of Fig. 15 discussed above, considerably more active sites will be found on the tube surface when the sampling time is increased, because most of the individual sites are active only once or twice within a video sequence of 500 ms (Fig. 15). On the other hand, the cumulative number N_{cum} found for 500 ms (449 cm^{-2} or 231 on 51.42 mm^2), will be close to the overall number of cavities within the micro structure of the surface that can ever be activated under the steady state conditions of this example, because increasing the time horizon from 40 to 500 ms led only to the double number of active sites. Similar results were found in another project of the joint program for a gold-plated copper tube with the same surface treatment [54].

It follows from these investigations of bubble formation without macro structure on the tubes, that it is not sufficient to analyze a simple site (on a non-technical or a technical heater surface) without the context of neighbouring sites, because this provides only a small part of the experimental information necessary to develop prediction methods for pool boiling heat transfer which should be based in future on the detailed (microscopic and macroscopic) events connected with vapour production to improve their validity beyond the range of experiments that were used.

In Figs. 17 and 18, examples of results for bubble formation on the Cu-tube *with the two macro structures* of Fig. 8 have been selected for boiling conditions corresponding to Figs. 15 and 16 as to reduced pressure p^* and heat flux q (see shaded areas in Fig. 19), but for a different boiling liquid (2-Propanol). At first glance, fluctuations and absolute values N_{sim} of simultaneously active sites are similar to the data without macro structure (cf. Fig. 17 and 16), and the same holds for the activation behaviour of the individual cavities, particularly within the simpler, secondary macro structure, where by far most of the cavities—macro cavities *or* cavities within the roughness structure—are active only once or twice during 500 ms (cf. Fig. 15, on the right, and Fig. 18, the two lower diagrams).

A more detailed comparison reveals, however, that there are significant differences in site activation between the two macro structures on the one hand (upper or lower diagrams of Fig. 18) or between macro cavities and cavities within the roughness structure, on the other (Fig. 18, cf. diagrams for *all* or only for *macro* cavities). The differences are:

- site activation of the *main* macro cavities is roughly four times as high as of the secondary (8.0 or 2.2), and almost twice as high as the activity of the roughness-sites in their neighbourhood (8.0 or 4.5), while
- the roughness-sites neighbouring the *secondary* macro cavities are almost 50% more active than the latter (3.0 or 2.2).

This is also reflected in the different numbers of simultaneously active sites (Fig. 17):

- There is almost the same number of *main* macro cavities active as roughness-cavities (macro: 6.7, all: 15.6), while
- the active *secondary* macro cavities constitute only about 25% of all active sites.

There are two reasons for the differences:

(1) The reentrant effects of the macro cavities within the main structure will trap a greater amount of vapour after a bubble has left than the secondary. Thus, bubble production is enhanced and therefore higher, because lower start-up superheat of the wall is needed, and this, in turn, will reduce activity of roughness-sites in their immediate vicinity.
(2) Roughness *within both kinds* of macro cavities has been reduced in the first production step, and *between the main* macro cavities in the second, while it has almost not been modified between the secondary macro cavities (see also Fig. 27 in Section 3).

The relative contribution of each of the two effects cannot be separated reliably with the experimental material available at present, but additional experiments with both kinds of roughness structure *without* macro cavities are planned (see Section 3).

Two more features of bubble formation after applying the macro structures can be observed: a certain ‘stabilizing’ effect which on the one hand, reduces the amplitudes of the temporal fluctuations of N_{sim} from the fine sandblasted surface without macro cavities (Fig. 16, bottom) in two steps to the secondary (Fig. 17, bottom) and then to the main structure (Fig. 17, top), and which on the other hand, increases bubble production at

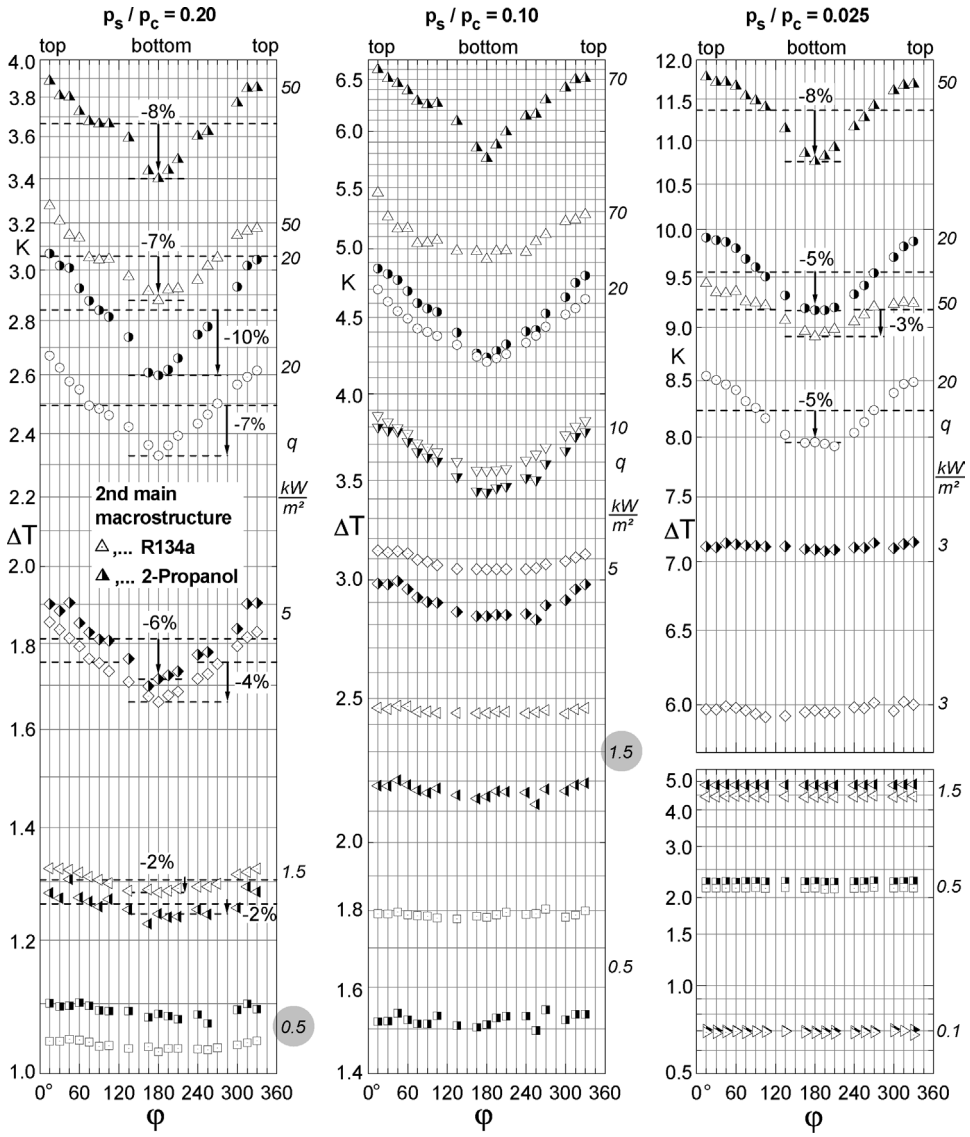

Fig. 22. Variation of local wall superheat ΔT with azimuthal angle φ and heat flux q at three pressures for R134a and 2-Propanol boiling on the Cu-tube with modified main macro structure.

individual sites, see the diagram for *all* cavities within the secondary domain in Fig. 18, compared with Fig. 15, on the right.

The second significant feature follows from Fig. 19 showing the marked increase of number of active sites in the area of the secondary structure (circles), compared to the fine sandblasted surface (squares) without macro structures (and compared to the main structure, triangles). Combined with the corresponding overall heat transfer results that yield systematic improvement of heat transfer from both enhanced surfaces over the fine sandblasted surface on the one hand, and small differences between the two former on the other, the effect seems to be analogous to the almost identical heat transfer coefficients, but marked differences of bubble production between the three fluids investigated with the fine sandblasted surface.

In the latter case, it could be proved by approximate calculations of evaporative and convective contributions of bubble formation to heat transfer that the experimental data from both domains (heat transfer or bubble production, respectively) are consistent with each other [31]. It is very likely that the seeming discrepancy between the data of Fig. 19 and the heat transfer results for the three surfaces [36] will be resolved in a similar way as soon as *complete* information on bubble formation from the enhanced surfaces is available, particularly on the bubble sizes.

3. New results from modified macro cavities

As the improvement of heat transfer from the main macro structure compared to the secondary structure was being comparatively small [36] for the first structure (of the 25.4 mm Cu-tube) shown in Figs. 8 and 12, the surface of the test tube was polished again, and after sandblasting, a second macro structure was applied which contained the same kind of secondary cavities, but main cavities with further reduced mouth widths, see Fig. 20, bottom, than for the first main structure (top). The heat transfer results for the main structure are shown in Fig. 21 by

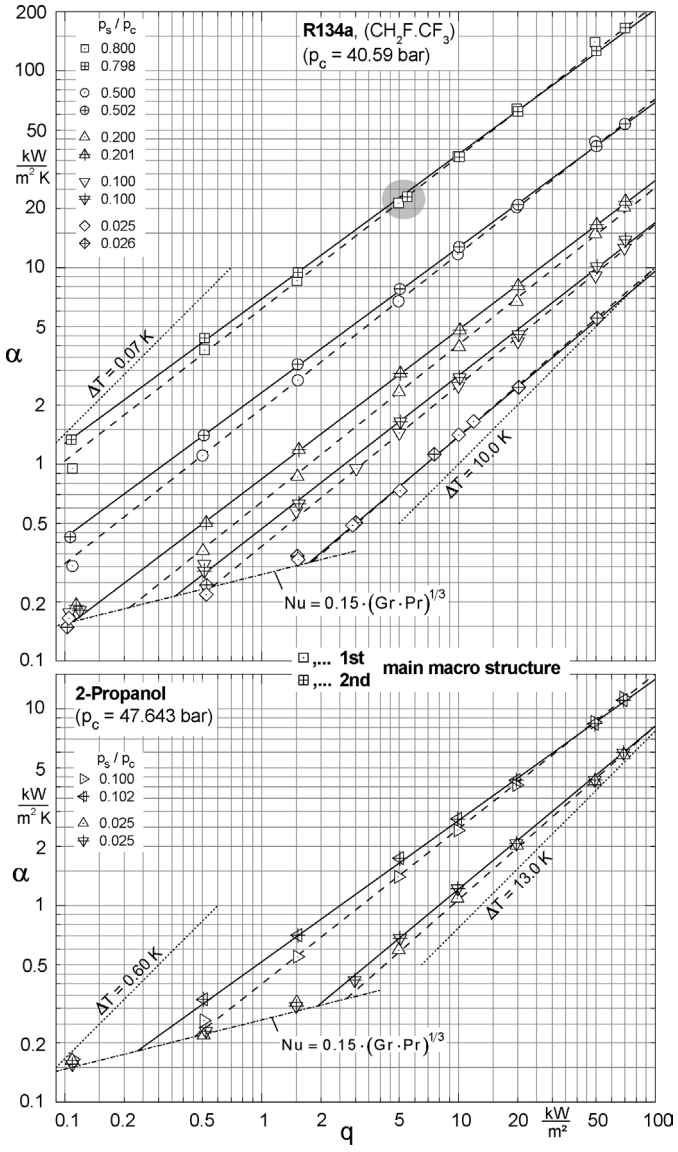

Fig. 23. Comparison of heat transfer results for the former (1st) main macro structure with data for the new structure with further reduced mouth width of the cavities at different heat fluxes and pressures. Top: R134a; bottom: 2-Propanol.

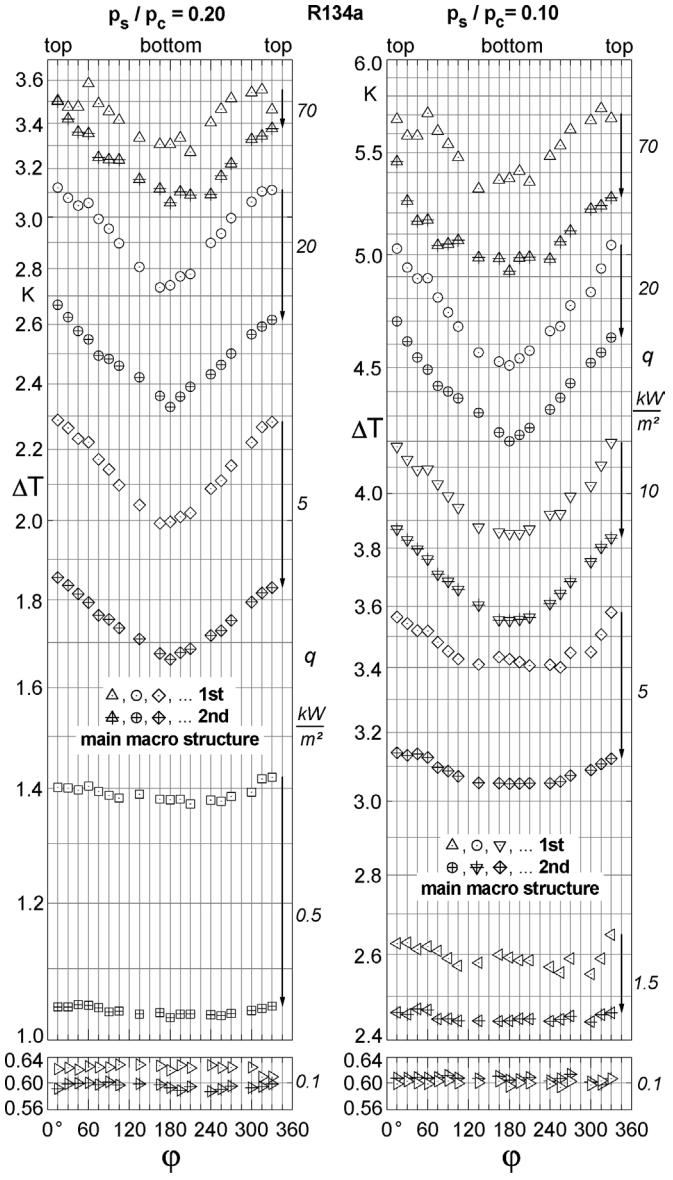

Fig. 24. Comparison of local wall superheat ΔT for first and second main macro structure with variation of heat flux q at $p^* = 0.1$ (right) and a higher pressure (left). Boiling liquid: R134a.

the *average* heat transfer coefficient $\alpha = q/\Delta T$ over the heat flux q for all experiments with R134a and 2-Propanol, and in Fig. 22 by the local wall superheat ΔT over azimuthal angle φ for the three pressures p^* investigated with both of the fluids. As had been expected, differences in α-values between the two fluids at corresponding *reduced* pressures p^* are small—for nucleate boiling and also for free convection without bubble formation—and only a slightly, but systematically weaker increase of α with q is observed for 2-Propanol than for R134a within the nucleate boiling region.

Local wall superheat is uniform for the whole circumference of the tube when no bubbles are formed (see Fig. 22, the three q-values of the lower diagram on the right) and at beginning nucleation (cf. e.g. squares on the left or triangles in the middle for 0.5 or 1.5 kW·m^{-2}, shaded), although α being already twice as high—or (the average) superheat half as high—in the latter case than without bubble formation (compare the shaded triangles in Fig. 21 and the dot-dashed lines).

Obviously, the local reduction in ΔT near the few active sites—being preferentially located on the lower parts of the tube—is compensated by the high thermal conductivity of the Cu-wall between the surface and the thermocouples located 1 mm below the surface, and by the fact, that the 'cooling effect' of the sliding bubbles is acting over a greater, coherent part of the circumference.

At *high* heat fluxes, the minimum of ΔT at the bottom of the tube is much more pronounced than without macro cavities for corresponding conditions, compare $q = 50$ and 20 kW·m^{-2} in the diagrams of Fig. 22 and Fig. 10 for $p^* = 0.2$ (on the left). In fact superheats at the bottom are between 7 and 10 % smaller than the average ΔT-value (Fig. 22), while without macro cavities no minimum can be observed at 50 kW·m^{-2} beyond the

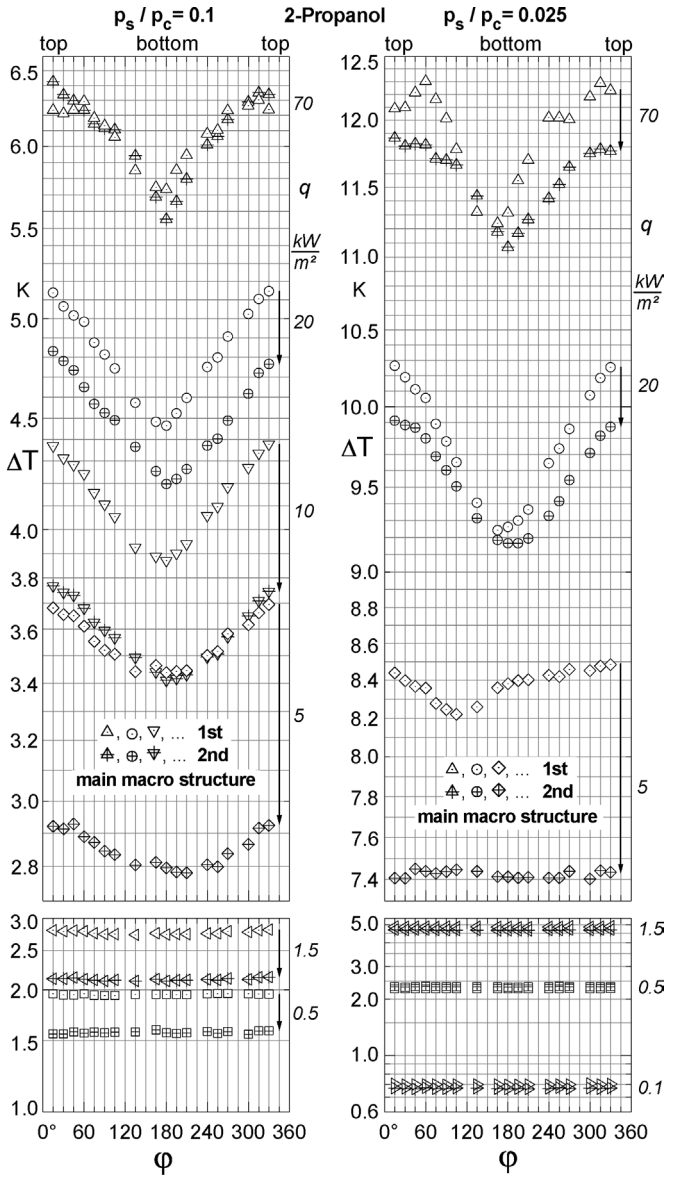

Fig. 25. Comparison of local wall superheat ΔT for first and second main macro structure with variation of heat flux q at $p^* = 0.1$ (left) and a lower pressure (right). Boiling liquid: 2-Propanol.

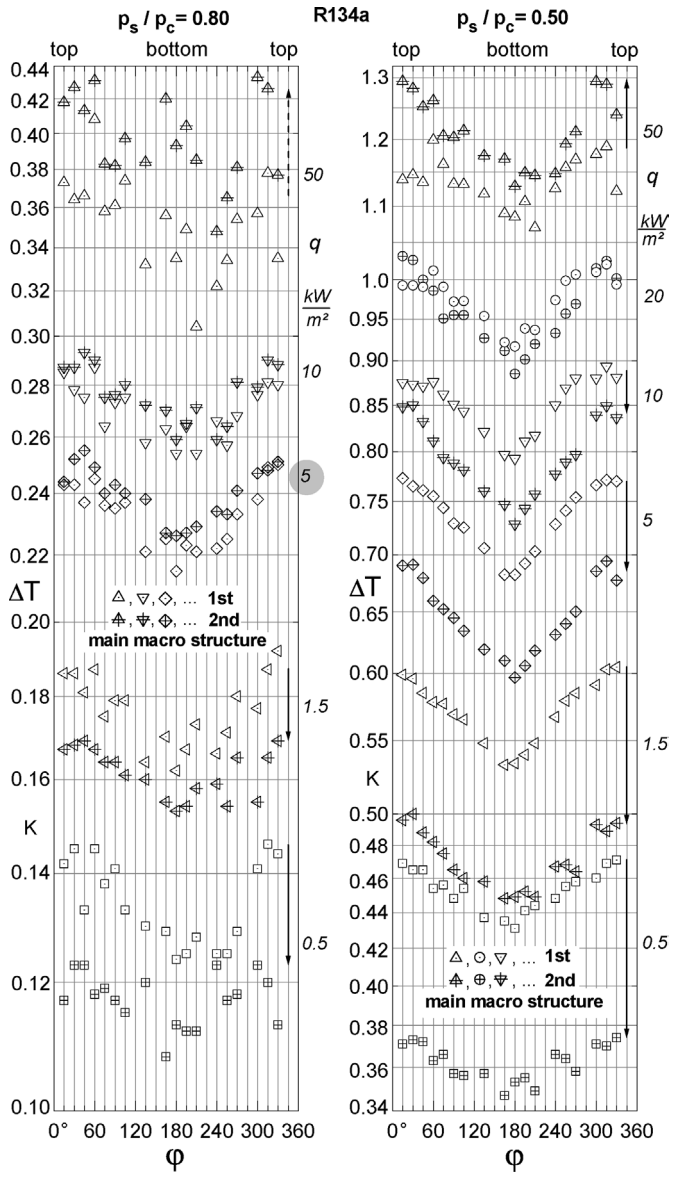

Fig. 26. Comparison of local wall superheat ΔT for first and second main macro structure with variation of heat flux q at two high reduced pressures. Boiling liquid: R134a.

ΔT-scatter of ± 0.1 K (or less than $\pm 3\%$). The distinguished ΔT-minimum at *high* heat fluxes is a further result of the stabilizing effect discussed above that seems to originate mainly from the bubbles sliding upwards with less lateral deviations than without the macro cavities that are equally distributed in a regular grid (similar to the difference between plain and conventionally finned tubes, see e.g. [6,40]). On the other hand, the relative decrease of ΔT towards the bottom of the tube is the same as without macro cavities at heat fluxes below approx. 10 kW·m^{-2}.

Having in mind that circumferential variations of ΔT may amount up to 10%, it should be noticed, that this has not been considered in the calculation of the *average* heat transfer coefficients α in Fig. 21 and 23. Instead, α has been calculated from the average superheats ΔT of the tube surface assuming purely radial heat flow within the tube and heat flux q to be independent of φ: $q = \text{const} = q_{\text{el}} = Q_{\text{el}}/(\pi \cdot D_a \cdot L_{\text{heated}})$. In reality, however, $\Delta T, \varphi$-variations as in Fig. 22 will cause heat flow within the wall from top to bottom of the tube, thus *reducing* the radial heat flux to the tube surface at the top and *increasing* it at the bottom. In [31], an example is given for the fine sand-blasted Cu-tube ($q_{\text{el}} = 20$ kW·m^{-2}, $p^* = 0.1$, $\Delta T_m = 5.62$ K, $(\Delta T_m - \Delta T_{\min})/\Delta T_m = 4.3\%$) that results in considerable variation of the local values of heat flux q and heat transfer coefficient α within the limits:

$$0.5 \leqslant q_{\text{loc}}/q_{\text{el}} \leqslant 1.3 \quad \text{and} \quad 0.45 \leqslant \alpha_{\text{loc}}/\alpha_{\text{m}} \leqslant 1.35$$

The *average* heat transfer coefficient $\alpha_{\text{loc},m}$ calculated from the *local* heat fluxes q_{loc}, however, differs from α_m (calculated from q_{el}) by less than one percent. This is in line with a systematic analysis for ΔT-variations up to values significantly higher than 10% in [55], where the influence on the average α-values

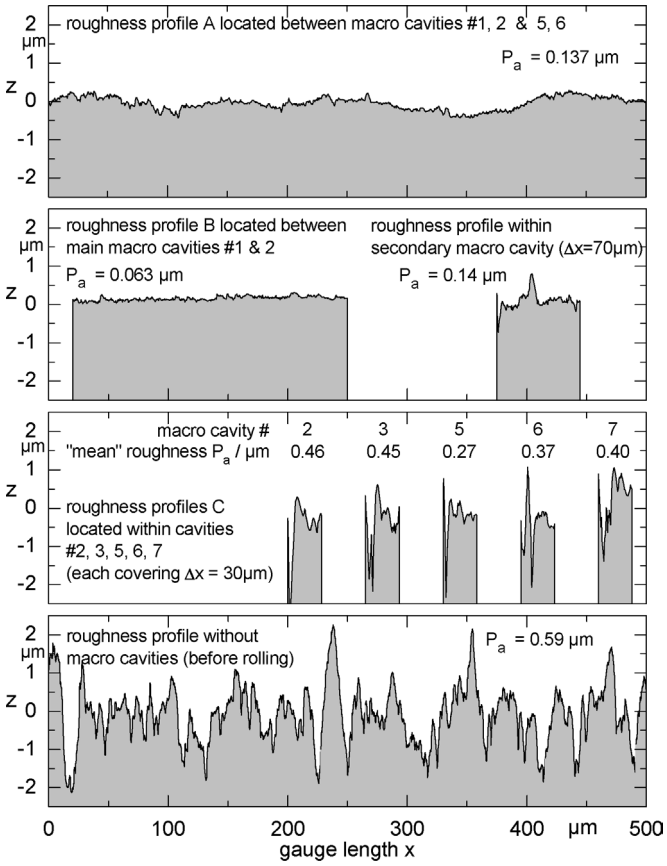

Fig. 27. Examples of roughness profiles for cavities at selected positions (see lower surface topography in Fig. 20) and comparison with a secondary macro cavity and with the roughness before rolling.

was always less than 3%. Therefore, calculation of heat transfer coefficients by $q = \text{const} = q_{\text{el}}$ has not been modified for simplicity reasons.

In Fig. 23, the heat transfer coefficients α of the second main macro structure are compared with the first within the whole pressure range investigated for R134a (top) and 2-Propanol (bottom; two pressures only, because the first structure had not been investigated at $p^* = 0.2$ for reasons of the high saturation temperature). As can be seen, the results differ very little at high heat fluxes within the whole pressure range, and improvement of heat transfer increases for the second main macro structure towards lower heat fluxes, particularly at intermediate reduced pressures (cf. solid and dashed interpolation lines). The quantitative differences can be recognized more clearly in the (more sensitive) representations of ΔT over φ in Figs. 24–26 for selected pressures and heat fluxes (some heat fluxes have been omitted for better visibility). The arrows on the right-hand side of the diagrams indicate (together with the α, q-diagrams) that the relative reduction of wall superheat (or improvement of heat transfer, respectively) is highest for $p^* = 0.1$ and 0.2 and for low heat fluxes near beginning nucleation, that also means comparatively small superheats of the wall and small densities of active nucleation sites on the surface. Obviously, the better vapour trapping within the macro cavities by their reduced mouth width is most effective when wall superheats get too small for activation of many micro cavities within the roughness structure.

At small reduced pressures, the effect is diminishing, see Fig. 25 on the right and Fig. 23, bottom, for 2-Propanol, and in the case of R134a, it has almost vanished completely, see Fig. 23, top. It seems that the macro cavities are too small and too close together to remain very effective with the increasing bubble sizes at these pressures. Towards high reduced pressures, $p^* = 0.5$ and 0.8, the effect is also becoming smaller (but for different reasons), and the slight improvement of heat transfer for intermediate to small reduced pressures at the highest heat fluxes investigated (see the arrows for 70 $\text{kW}\cdot\text{m}^{-2}$ in Figs. 24 and 25) has even turned to the opposite, see the arrows for 50 $\text{kW}\cdot\text{m}^{-2}$ in Fig. 26. This indicates that enhanced vapour trapping in the 2nd kind of main macro cavities is negative already, because it represents an additional heat transfer resistance under these conditions with excellent heat transfer coefficients (40 to 140 $\text{kW}\cdot\text{m}^{-2}\cdot\text{K}^{-1}$, see Fig. 23, top), but slow movement of the vapour phase because of the tiny bubble sizes and small vapour/liquid density difference that impedes reflux of liquid at high vapour production rates.

On the other hand, improvement of heat transfer by the smaller mouth width becomes effective again with decreasing vapour production at smaller superheats or heat fluxes, see Fig. 26, bottom. And as already discussed in the comparison of Figs. 22 and 10 above, the stabilizing effect of the regular grid of macro cavities on local heat transfer via the 'stratified' upflow of sliding bubbles can be observed, that reduces the data scatter and accentuates the $\Delta T, \varphi$-minimum, compare the triangles for $p^* = 0.8$, $q = 10$ $\text{kW}\cdot\text{m}^{-2}$ in Fig. 26 on the left and the triangles for the corresponding boiling conditions at the bottom of Fig. 10, on the right. This implies that (at least) a great part of the irregular scatter in the latter case is not caused by arriving at the experimental limit of error, but by irregularities of local bubble production without the stabilizing effect of the macro cavities.

In this very detailed quantitative analysis of small ΔT-differences between the 1st and 2nd main macro structure (or without macro cavities respectively), it has to be taken into account that comparisons should always be done at *exactly the same* heat fluxes. This is not always the case in Figs. 24–26 because the individual experimental data of the thermocouples have been used. If pertaining experimental q-values are differing, this may be misleading, as is demonstrated for $p^* = 0.8$, $q = 5$ $\text{kW}\cdot\text{m}^{-2}$ (shaded in Figs. 23 and 26). The higher ΔT-values in Fig. 26 (rhombi with cross)—signalizing *worse* heat transfer if heat fluxes were the same—are caused only by the slightly higher experimental heat flux in case of the second main macro structure (square with cross, shaded in Fig. 23), because moving the symbol along the interpolation line would result in congruent symbols or exactly the same average ΔT-value in both cases.

Analysis of bubble formation at the end of Section 2 revealed that important parts are still missing for the first macro structure, and the same holds for the second structure to a higher extent. Both investigations are currently under way, and in addition, measurements of heat transfer and bubble formation with-

Standardized roughness parameters according to DIN EN ISO 4287

	P_a [µm]	P_q [µm]	P_p [µm]	$P_{p,m}$ [µm]	P_t [µm]	P_Z [µm]
mean*	0.091	0.117	0.356	0.229	0.841	0.535
max.	0.178	0.208	1.104	0.467	1.788	0.975
min.	0.044	0.056	0.169	0.141	0.331	0.271
σ	0.021	0.026	0.118	0.046	0.229	0.128

* Number of runs: 1000, near thermocouple #28 ($\phi = 275°$).
Topography (enlargement $(z/x) = 36$).

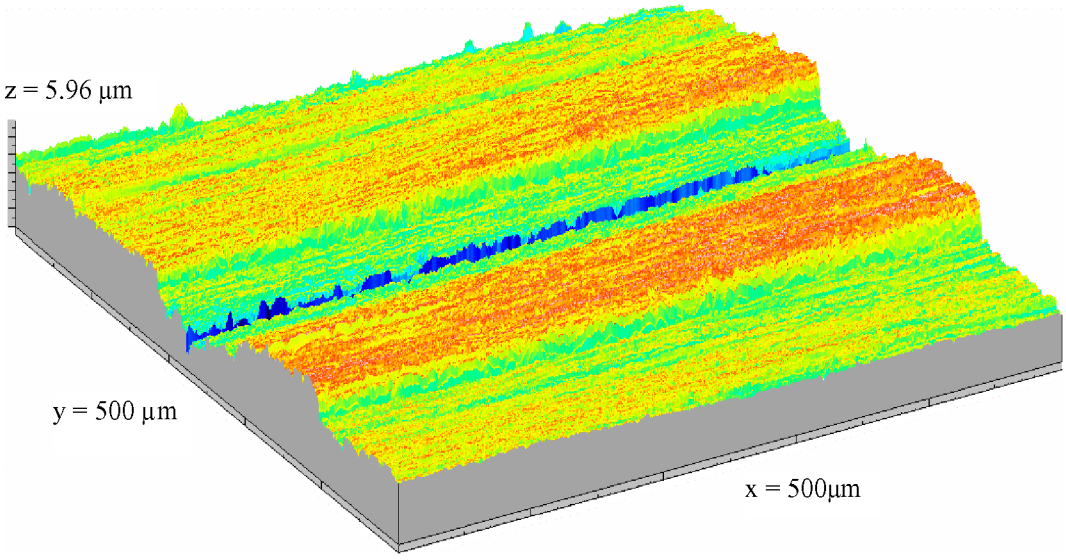

Fig. 28. Topography and standardized roughness parameters after rolling the tube in the same way as for application of second main macro structure (corresponding to profiles A & B in Fig. 27).

out macro cavities, but modified roughness of the tube surface are being prepared, that follow from the smoothing effect of the second rolling process in the production of the main structures, see Fig. 27 in connection with Fig. 20, bottom.

The roughness profiles A (located between the two rows of macro cavities in Fig. 20, bottom) and B (located between cavities #1 and 2 in Fig. 20) demonstrate that the original roughness of the sandblasted surface existing on the tube surface before rolling and between the secondary macro cavities after the first rolling step (Fig. 27, bottom) has been flattened severely (from $P_a = 0.59$ µm to approx. 0.1 µm). Similar roughness levels are found at the bottom of each macro cavity, see the shorter run for one of the secondary macro cavities in Fig. 27, second diagram from top, on the right. Within the *main* macro cavities, roughness seems to be higher (Fig. 27, profiles *C* in the third diagram from top), but these results could be influenced by their very short gauge lengths ($\Delta x = 30$ µm) and by the sharp peaks on the left that may be electronic reactions of the sensor caused by the sharp change of the slope at the edge of the macro cavities. Instead, it is very likely that roughness within main and secondary macro cavities is the same, because both kinds of macro cavities have been formed in the same (first) rolling step, and the following step should not have modified *the bottom* of the main macro cavities. (It should be mentioned here, that a new sandblasting procedure was applied before rolling the new macro structure discussed in Section 3, in order to obtain a somewhat higher roughness level and broader size distribution of the micro cavities that are closer to common surface roughness in practice than the fine sandblasted one used before.)

Following from the results of Fig. 27, it appears to be important that bubble formation and heat transfer on the tube surface *with* macro cavities should not only be compared with the results for the original sandblasted surface before rolling, but also with a surface containing the roughness structure produced by the rolling process, but *without* adding macro cavities. This procedure has been applied to the area on the tube assigned for the main macro structure (30 mm in length, see Fig. 9), and the topography and the standardized roughness parameters in Fig. 28 demonstrate that the roughness structure achieved corresponds to the results of Fig. 27 between the main macro cavities (and within the macro cavities). Measurements of heat transfer and bubble formation for this surface will start now.

4. Conclusions

The coherent new data on heat transfer and bubble formation from the same evaporator surfaces with technically relevant roughness structures and with high accuracy of the local results gained from growing, departing and sliding bubbles have given new insights into the manifold interactions between neighbouring bubbles and nucleation sites and into their contributions to heat transfer from surfaces *with* and also *without* surface modifications for heat transfer enhancement. The results are suitable to interpret the basic convective and evaporative processes which produce heat transfer enhancement in nucleate pool boil-

ing. At present it is too early, however, to draw final conclusions for the project discussed here, because only a few examples of the new experimental material on bubble formation have been analyzed so far and measurements of heat transfer and bubble formation for the last surface configuration are still missing.

Acknowledgements

The authors highly appreciate financial support of Deutsche Forschungsgemeinschaft (DFG) in the frame of the Joint Research Program on fundamentals of boiling heat transfer. The authors are also grateful to Fa. Solvay Deutschland GmbH for supplying the refrigerant and to the manufacturer of the macro structures, Wieland-Werke AG, Ulm and to their Technical Staff for positioning the structures on the tubes with high accuracy.

References

[1] S. Caplanis, Blasensieden an Hochleistungsrohren, PhD thesis, Universität (GH) Paderborn, 1997.
[2] R.L. Webb, The evolution of enhanced surface geometries for nucleate boiling, Heat Transfer Engrg. 2 (1981) 46–69.
[3] S.B. Memory, D.C. Sugiyama, P.J. Marto, Nucleate pool boiling of R114 and R114-oil mixtures from smooth and enhanced surfaces—I. Single tubes, Int. J. Heat Mass Transfer 38 (1995) 1347–1361.
[4] J.R. Thome, Enhanced Boiling Heat Transfer, Hemisphere, Washington, DC, 1990.
[5] R.L. Webb, Pool boiling, in: Principles of Enhanced Heat Transfer, Wiley, New York, 1994, pp. 311–372 (Chapter 11).
[6] P. Hübner, Zum Wärmeübergang beim Blasensieden an Rippenrohren, PhD thesis, Universität (GH) Paderborn, 2000.
[7] R. Mertz, Beitrag zum Behältersieden von Kohlenwasserstoffen an Rohren mit hinterschnittenen Oberflächen, PhD thesis, Universität Stuttgart, 2001.
[8] R.M. Manglik, A.E. Bergles, Enhanced heat and mass transfer in the new millennium: A review of the 2001 literature, J. Enhanced Heat Transfer 11 (2004) 87–118;
Cf. also: A.E. Bergles, High-flux processes through enhanced heat transfer, in: Proc. 5th Int. Boiling Heat Transfer Conf., Montego Bay, Jamaica, 2003.
[9] P.S. O'Neill, C.F. Gottzman, J.W. Terbot, Novel heat exchanger increases cascade cycle efficiency for natural gas liquefaction, in: K.D. Timmerhaus (Ed.), Cryogenic Engineering, Plenum, New York, 1972, pp. 420–437.
[10] W. Nakayama, T. Daikoku, H. Kuwahara, T. Nakajima, Dynamic model of enhanced boiling heat transfer on porous surfaces, part I: Experimental investigation, part II: Analytical modeling, J. Heat Transfer 102 (1980) 445–456;
Cf. also: W. Nakayama, T. Daikoku, T. Nakajima, Effects of pore diameters and system pressure on saturated pool nucleate boiling heat transfer from porous surfaces, J. Heat Transfer 104 (1982) 286–291.
[11] K. Nishikawa, T. Ito, K. Tanaka, Augmented heat transfer by nucleate boiling at prepared surfaces, in: Proc. ASME–JSME Thermal Engineering Conf., vol. 1, 1983, pp. 387–393;
Cf. also: K. Nishikawa, T. Ito, Augmentation of nucleate boiling heat transfer by prepared surfaces, in: T. Mizushina, W.J. Yang (Eds.), Heat Transfer in Energy Problems, Hemisphere, New York, 1982, pp. 111–118.
[12] M.D. Xin, Y.D. Chao, Analysis and experiment of boiling heat transfer on T-shaped finned surfaces, in: AIChE paper, 23rd Nat. Heat Transfer Conf., Denver, CO, 1985.
[13] Z.H. Ayub, A.E. Bergles, Pool boiling from GEWA surfaces in water and R113, Wärme- und Stoffübertragung 21 (1987) 209–219.
[14] S.A. Kovalev, S.L. Solov'yev, O.A. Ovodkov, Theory of boiling heat transfer on a capillary porous surface, in: Proc. 9th Int. Heat Transfer Conf., vol. 2, 1990, pp. 105–110.
[15] D.Y. Wang, J.G. Cheng, H.J. Zhang, Pool boiling heat transfer from T-finned tubes at atmospheric and super-atmospheric pressures, in: Phase Change Heat Transfer, in: ASME HDT, vol. 159, 1991.
[16] R.L. Webb, S.I. Haider, An analytical model for nucleate boiling on enhanced surfaces, in: V.J. Dhir, A.E. Bergles (Eds.), Pool and External Flow Boiling, ASME, New York, 1992, pp. 345–360.
[17] Y. Zhang, H. Zhang, Boiling heat transfer from a thin powder porous layer at low and moderate heat flux, in: X.-J. Chen, T.N. Veziroglu, C.L. Teen (Eds.), Multiphase Flow and Heat Transfer, 2nd Int. Symposium, vol. 1, Hemisphere, New York, 1992, pp. 358–366.
[18] Z. Lin, T. Ma, Z. Zhang, Pool boiling on porous surfaces with microgrooves, in: Proc. 10th Int. Heat Transfer Conf., vol. 5, 1994, pp. 111–116.
[19] S.I. Haider, R.L. Webb, A transient micro-convection model of nucleate pool boiling, Int. J. Heat Mass Transfer 40 (1997) 3675–3688.
[20] M.H. Saidi, M. Ohadi, M. Souhar, Enhanced pool boiling of R123 refrigerant on two selected tubes, Appl. Thermal Engrg. 19 (1999) 885–895.
[21] L.-H. Chien, R.L. Webb, A nucleate boiling model for structured enhanced surfaces, Int. J. Heat Mass Transfer 41 (1998) 2183–2195.
[22] S.G. Liter, M. Kaviany, Pool boiling CHF enhancement by modulated porous-layer coating: theory and experiment, Int. J. Heat Mass Transfer 44 (2001) 4287–4311.
[23] D. Gorenflo, A. Luke, E. Danger, Interactions between heat transfer and bubble formation in nucleate boiling, in: Proc. 11th Int. Heat Transfer Conf., Kyongju, Korea, vol. 1, 1998, pp. 149–174.
[24] P. Sokol, P. Blein, D. Gorenflo, W. Rott, H. Schömann, Pool boiling heat transfer from plain and finned tubes to Propane and Propylene, in: Heat Transfer 1990, Proc. 9th Int. Heat Transfer Conf., Jerusalem, vol. 2, 1990, pp. 75–80.
[25] D. Gorenflo, P. Sokol, S. Caplanis, Zum Wärmeübergang beim Blasensieden von Kohlenwasserstoffen und Halogen-Kältemitteln an einem Glattrohr und einem Hochleistungs-Rippenrohr, Wärme- und Stoffübertragung 26 (1991) 273–281.
[26] D. Gorenflo, S. Caplanis, W. Künstler, Enhanced pool boiling heat transfer to new refrigerants, in: Proc. Int. Inst. Refrig. Comm. B1/B2 Conf., Ghent, 1993-2, pp. 327–334.
[27] P. Hübner, W. Künstler, Pool boiling heat transfer on finned tubes: influence of surface roughness and shape of the fins, Int. J. Refrig. 20 (1997) 575–582.
[28] H. Thaler, A. Luke, Wärmeübergang beim Blasensieden in Propan an neuartigen, plasmagespritzten Obenflächen, Paper presented at Annual Nat. Meeting of VDI-GVC Heat & Mass Transfer Committee, Bamberg, 2001, Paper #15.
[29] K. Bier, H.R. Engelhorn, D. Gorenflo, Heat transfer at burnout and Leidenfrost points for pressures up to critical, in: E. Hahne, U. Grigull (Eds.), Heat Transfer in Boiling, Hemisphere, Washington, DC, 1977, pp. 85–98;
Cf. also: D. Gorenflo, Wärmeübergang bei Blasensieden, Filmsieden und einphasiger freier Konvektion in einem großen Druckbereich, Abh. deutsch. Kälte- und Klimatechn. Ver., vol. 22, C.F. Müller-Verlag, Karlsruhe, 1977;
Cf. also: D. Gorenflo, H.E. Alpay, Burnout heat transfer to SF_6/R13B1-mixtures at near-critical saturation pressures, in: Proc. 16th Int. Congr. Refrig., Paris, vol. II, 1983, pp. 155–162.
[30] D. Gorenflo, U. Chandra, S. Kotthoff, A. Luke, Influence of thermophysical properties on pool boiling heat transfer of refrigerants, Int. J. Refrig. 27 (2004) 492–502.
[31] E. Danger, Wärmeübergang und Blasenbildung beim Sieden, PhD Thesis, Universität Paderborn, 2004.
[32] A.E. Bergles, M.C. Chyu, Characteristics of nucleate pool boiling from porous metallic coatings, J. Heat Transfer 104 (1982) 279–285.
[33] W. Fath, Wärmeübergangsmessungen an Glatt- und Rippenrohren in einer Standardapparatur für Siedeversuche, PhD thesis, Universität (GH) Paderborn, 1986.
[34] A.D. Pinto, S. Caplanis, P. Sokol, D. Gorenflo, Variation of hysteresis phenomena with saturation pressure and surface roughness, in: V.J. Dhir, A.E. Bergles (Eds.), Proc. Pool and External Flow Boiling Conf. Santa Barbara, ASME, New York, 1992, pp. 37–42.
[35] M.E. Poniewski, Peculiarities of boiling heat transfer on capillary-porous coverings, Int. J. Thermal Sci. 43 (2004) 431–442.
[36] D. Gorenflo, A. Luke, E. Danger, U. Chandra, S. Kotthoff, Heat transfer and bubble formation of Propane boiling on tubes with basic surface modifications for enhancement, in: Proc. 5th Gustav Lorentzen Conf., Int. Inst. Refrig., Guangzhou (China), 2002, pp. 363–370.

[37] K. Bier, J. Goetz, D. Gorenflo, Zum Einfluß des Umfangswinkels auf den Wärmeübergang beim Blasensieden an horizontalen Rohren, Wärme- und Stoffübertragung 15 (1981) 159–169;
Cf. also: J. Goetz, Entwicklung und Erprobung einer Normapparatur zur Messung des Wärmeübergangs beim Blasensieden, PhD thesis, Universität (TH) Karlsruhe, 1980.

[38] P. Sokol, Untersuchungen zum Wärmeübergang beim Blasensieden an Glatt- und Rippenrohren mit grossem Aussendurchmesser, PhD thesis, Universität (GH) Paderborn, 1994.

[39] P. Kaupmann, D. Gorenflo, A. Luke, Pool boiling heat transfer on horizontal steel tubes with different diameters, Multiphase Sci. Technol. 12 (2001) 14–26.

[40] P. Hübner, D. Gorenflo, A. Luke, Circumferential temperature distributions on plain and finned tubes in pool boiling, in: Proc. 3rd Conf. Compact Heat Exchangers, Davos, 2001, pp. 383–490.

[41] D. Gorenflo, W. Fust, A. Luke, E. Danger, U. Chandra, Pool boiling heat transfer from tubes with basic surface modifications for enhancement—design of the test tubes and first measurements, in: Proc. Third European Thermal Sciences Conf., Heidelberg, vol. 2, 2000, pp. 743–748.

[42] A. Luke, E. Danger, Size distribution of active and potential nucleation sites on horizontal evaporator tubes, in: Proc. Int. Inst. Refrig. Comm. B1 Conf., Paderborn, 2001-5, pp. 396–403.

[43] A. Luke, E. Danger, F. Sander, Vergleich aktiver und potentieller Blasenkeimstellen beim Sieden am horizontalen Verdampferrohr, DKV-Tagungsbericht 28 (II.1) (2001) 111–122.

[44] D. Gorenflo, E. Danger, A. Luke, S. Kotthoff, U. Chandra, C. Ranganayakulu, Bubble formation with pool boiling on tubes with or without basic surface modifications for enhancement, Int. J. Heat Fluid Flow 25 (2004) 288–297.

[45] E. Danger, U. Chandra, D. Gorenflo, A. Beutler, Basic modifications of the heated surface for enhancement of pool boiling heat transfer, in: Proc. Int. Inst. Refrig. Comm. B1 Conf., Paderborn, 2001-5, pp. 380–387.

[46] J. von Hardenberg, D.B.R. Kenning, H. Xing, L.A. Smith, Identification of nucleation site interactions, Int. J. Heat Fluid Flow 25 (2004) 298–304.

[47] D.B.R. Kenning, T. Kono, M. Wienecke, Investigation of boiling heat transfer by liquid crystal thermography, Exp. Therm. Fluid Sci. 25 (2001) 219–229.

[48] D.B.R. Kenning, Y. Yan, Pool boiling heat transfer on a thin plate: features revealed by liquid crystal thermography, Int. J. Heat and Mass Transfer 39 (1996) 3117–3137.

[49] B. Mikic, W. Rohsenow, A new correlation of pool boiling data including the effect of heating surface characteristics, J. Heat Transfer 91 (1969) 245–250.

[50] C.-Y. Han, P. Griffith, The mechanism of heat transfer in nucleate pool boiling, Parts I and II, Int. J. Heat Mass Transfer 8 (1965) 887–914.

[51] A. Luke, D. Gorenflo, Heat transfer and size distribution of active nucleation sites in boiling propane outside a tube, Int. J. Thermal Sci. 39 (2000) 919–930.

[52] M. Weckesser, Untersuchungen zur Blasenbildung beim Sieden in freier Konvektion, PhD thesis, Universität Karlsruhe (TH), 1990.

[53] E. Baumhögger, D. Gorenflo, Internal report of ThEt, Thermodynamik und Energietechnik, Universität Paderborn, 2003, Unpublished.

[54] G. Barthau, E. Hahne, Nucleate pool boiling of R134a on gold-plated copper test tube, in: Proc. Int. Inst. Refrig. Comm. B1 Conf., Paderborn, 2001-5, pp. 372–379.

[55] P. Kaupmann, Durchmessereinfluss und örtlicher Wärmeübergang beim Blasensieden an horizontalen Stahlrohren, PhD thesis, Universität (GH) Paderborn, 1999.